Electronic Supplementary Material (ESI) for ChemComm.
This journal is © The Royal Society of Chemistry 2022

Electronic Supplementary Information

5-Thiaporphyrinium Cation: Effect of Sulphur Incorporation on Excited State Dynamics

Asahi Takiguchi,[a] Naoto Inai,[b] Seongsoo Kang,[c] Masaya Hagai,[d] Seokwon Lee,[c] Takeshi Yanai*[b,e] Dongho Kim*[c] and Hiroshi Shinokubo*[a]

[a] *Department of Molecular and Macromolecular Chemistry, Graduate School of Engineering, Nagoya University, Chikusa-ku, Nagoya, Aichi 464-8603, Japan.*

[b] *Department of Chemistry, Graduate School of Science, Nagoya University, Furo-cho, Chikusa-ku, Nagoya, Aichi 464-8602, Japan*

[c] *Department of Chemistry, Spectroscopy Laboratory for Functional π-Electronic Systems Yonsei University, Seoul 03722, South Korea*

[d] *Department of Chemistry, School of Science, Nagoya University, Furo-cho, Chikusa-ku, Nagoya, Aichi 464-8602, Japan*

[e] *Institute of Transformative Bio-Molecules (WPI-ITbM), Nagoya University, Furo-cho, Chikusa-ku, Nagoya, Aichi 464-8602, Japan*

E-mail: yanait@chem.nagoya-u.ac.jp; dongho@yonsei.ac.kr; hshino@chembio.nagoya-u.ac.jp

Table of Contents

1. Instrumentation and Materials

^1H NMR (500 MHz), ^{13}C NMR (126 MHz), and ^{19}F NMR (471 MHz) spectra were recorded on a Bruker AVANCE III HD 500 spectrometer. Chemical shifts were reported as the delta scale in ppm relative to $CHCl_3$ ($\delta = 7.26$ ppm) for ^1H NMR, $CDCl_3$ ($\delta = 77.16$ ppm) for ^{13}C NMR, and hexafluorobenzene ($\delta = -161.64$ ppm) for ^{19}F NMR. UV/Vis/NIR absorption spectra were recorded on a Shimadzu UV-2550 spectrometer or JASCO V 670 spectrometer. Emission spectra were recorded on a JASCO FP-8500 spectrometer. Absolute fluorescence quantum yields were measured by the photon-counting method using an integration sphere. Absolute fluorescence quantum yields at 77 K were determined with a Hamamatsu Photonics C9920-03G calibrated integrating sphere system with A11238-01. Melting points were measured on a Stanford Research Systems OptiMelt MPA100. High-resolution atmospheric pressure chemical ionization time-of-flight (APCI-TOF) mass spectra were taken on a Bruker micrOTOF instrument using a positive ionization mode. X-ray data were obtained using a Rigaku CCD diffractometer (Saturn 724 with MicroMax-007) with Varimax Mo optics and a Bruker D8 QUEST X-ray diffractometer with an IμS microfocus X-ray source and a PHOTON II detector. Cyclic voltammograms were recorded using an ALS electrochemical analyzer 612C. Measurements were performed in freshly distilled dichloromethane with tetrabutylammonium hexafluorophosphate (0.1 M) as the electrolyte. A three-electrode system was used. The system consisted of a glassy carbon working electrode, a platinum wire, and $Ag/AgClO_4$ as the reference electrode. The scan rate was 100 mVs^{-1}. The measurement was performed under nitrogen atmosphere. All potentials are referenced to the potential of ferrocene/ferrocenium cation couple. All calculations were carried out using the Gaussian 09 software package.[1] Initial geometries for the calculations were obtained from the X-ray crystal structures. The ethyl substituents were replaced with hydrogen atoms and the counter ion was not included to reduce the calculation cost. The calculations were performed by the density functional theory (DFT) method with the restricted CAM-B3LYP[2] level, employing basis sets 6-311+G(2d,p) for C, H, N, and S and SDD for Zn. The solvent effect (dichloromethane) was considered by the polarizable continuum model (PCM) method.[3] Zero-point energy and thermal energy corrections were conducted at the CAM-B3LYP/6-311+G(2d,p) level, and the sums of electronic and thermal free energies were obtained. The zero-point energies were not scaled, and the enthalpic corrections were made at 298.15 K. Oxaporphyrin **1-Zn** was prepared according to the literature.[4] Unless otherwise noted, materials obtained from commercial suppliers were used without further purification. Preparative separations were performed by silica-gel column chromatography (Wakogel$^{®}$ C-300) and amino-functionalized silica-gel column chromatography (Fuji Silysia Chemical NH-DM1020).

2. Experimental Procedures and Compound Data

2,3,7,8,12,13,17,18-Octaethyl-21*H*,23*H*,24*H*-19-oxo-1-thioxo-bilin: 2

A Schlenk tube containing **1-Zn** (0.14 g, 98 µmol) and anhydrous sodium sulfide (23 mg, 0.30 mmol) was evacuated and then refilled with N_2. To the tube, 20 mL of the dry tetrahydrofuran was added and stirred at room temperature for 0.5 h. After evaporation, the resulting mixture was redissolved in dichloromethane, washed with 1 M hydrochloric acid, and water twice. The combined organic layers were dried over anhydrous sodium sulfate. After evaporation, the residue was purified by amino-functionalized silica-gel column chromatography (dichloromethane as eluent) and silica-gel column chromatography (dichloromethane as eluent). After recrystallization from dichloromethane/hexane, **2** (55 mg, 96 µmol, 98% yield) was obtained as dark purple crystals.

M.p. 196 °C (decomposed); ^{1}H NMR (500 MHz, $CDCl_3$, 25 °C): δ = 9.09 (br-s, 1H, NH), 7.62 (br-s, 2H, NH), 6.85 (s, 1H, *meso*), 6.22 (s, 1H, *meso*), 6.13 (s, 1H, *meso*), 2.70–2.49 (m, 14H, ethyl), 2.18 (q, J = 7.6 Hz, 2H, ethyl), 1.34 (t, J = 7.7 Hz, 3H, ethyl), 1.29 (t, J = 7.7 Hz, 3H, ethyl), 1.25–1.17 (m, 12 H, ethyl), 1.11 (t, J = 7.6 Hz, 3H, ethyl), 1.02 (t, J = 7.6 Hz, 3H, ethyl) ppm; ^{13}C NMR (126 MHz, $CDCl_3$, 25 °C): δ = 191.8, 172.1, 150.6, 148.7, 147.0, 144.2, 142.5, 142.4, 142.0, 141.9, 141.1, 140.5, 138.9, 135.6, 134.6, 133.0, 113.4, 97.8, 96.6, 18.4, 18.4, 18.1, 18.0, 17.9, 17.8, 17.2, 17.1, 17.0, 16.4, 16.1, 16.0, 15.8, 14.8, 13.4 ppm; UV/Vis (CH_2Cl_2): $\lambda_{\max}$ (ε [M^{-1} cm^{-1}]) = 320 (3.0×10^4), 410 (5.2×10^4), 708 (1.2×10^4) nm; HRMS (APCI-TOF, positive mode): $[M+H]^+$ Calcd for $C_{35}H_{46}N_4OS$ 571.3465; Found 571.3422.

Free-base 2,3,7,8,12,13,17,18-octaethyl-5-thiaporphyrinium tetrakis[3,5-bis(trifluoromethyl)phenyl]borate: 3-2H

A Schlenk tube containing **2** (29 mg, 50 µmol) was evacuated and then refilled with nitrogen gas. To the tube, dry and degassed dichloromethane (10 mL) and trifluoromethanesulfonic anhydride (16 µL, 0.10 mmol) were added. The mixture was stirred at room temperature for 0.5 h. The mixture was washed with water and dried over anhydrous sodium sulfate. After removing the solvent, sodium tetrakis[3,5-bis(trifluoromethyl)phenyl]borate (54 mg, 61 µmol) and dichloromethane (10 mL) were added to the residue. The mixture was stirred at room temperature for 5 min. The resulting mixture was washed with water three times and dried over anhydrous sodium sulfate. After removing the solvent, the residue was purified by silica-gel column chromatography (dichloromethane/hexane = 1/1 as eluent) to afford **3-2H** (22 mg, ca. 15 µmol) along with ca. 1% of **1-2H** in 30% yield as a dark purple solid. After short column chromatography with amino-functionalized silica-gel (dichloromethane as eluent) to remove **1-2H**, **3-2H** was obtained in 21% yield (15 mg, 10 μmol).

M.p. 186 °C (decomposed); ^{1}H NMR (500 MHz, $CDCl_3$, 25 °C): δ = 10.26 (s, 1H, *meso*), 10.24 (s, 2H, *meso*), 7.70 (s, 8H, Ar-*o*), 7.47 (s, 4H, Ar-*p*), 4.03–3.93 (m, 16H, ethyl), 1.90–1.84 (m, 24H, ethyl), –1.05 (s, 2H, NH) ppm; ^{13}C NMR (126 MHz, $CDCl_3$, 25 °C): δ = 161.8 (q, J = 50 Hz, Ar-*ipso*), 149.6, 148.6, 148.4, 147.5, 147.4, 145.6, 144.3, 142.1, 134.9 (s, Ar-*o*), 129.0 (q, J = 32 Hz, Ar-*m*), 124.7 (q, J = 273 Hz, CF_3), 117.5 (t, J = 3.7 Hz, Ar-*p*), 111.4, 108.9, 19.9, 19.7, 19.5, 19.4, 18.5, 18.3, 18.2, 17.7 ppm; ^{19}F NMR (471 MHz, $CDCl_3$, 25 °C): δ = –62.4 (24F) ppm; UV/Vis (CH_2Cl_2): $\lambda_{\max}$ (ε [M^{-1} cm^{-1}]) = 310 (3.0×10^{4}), 392 (1.1×10^{5}), 671 (5.6×10^{4}) nm; FL (λ_{ex} = 550 nm, CH_2Cl_2): $\lambda_{\max}$ (nm) = 686 (<1%); HRMS (APCI-TOF, positive mode): [thiaporphyrinium]$^{+}$ Calcd for $C_{35}H_{45}N_4S$ 553.3359; Found 553.3354; HRMS (APCI-TOF, negative mode): [$BAr^{F}{}_4$]$^{-}$ Calcd for $C_{32}H_{12}{}^{11}BF_{24}$ 863.0649; Found 863.0661.

Zinc 2,3,7,8,12,13,17,18-octaethyl-5-thiaporphyrinium tetrakis[3,5-bis(trifluoromethyl)phenyl]borate: 3-Zn

A round-bottomed flask containing **3-2H** (14 mg, 10 μmol) and bis(2,4-pentanedionato)zinc(II) (13 mg, 50 μmol) was charged with tetrahydrofuran (5 mL). The mixture was stirred at room temperature for 1 h. After evaporation, the residue was purified by silica-gel column chromatography (dichloromethane as eluent). After recrystallization from dichloromethane/hexane, **3-Zn** (14 mg, 9.6 μmol, 96% yield) was obtained as dark purple crystals.

M.p. 144 °C (decomposed); ^{1}H NMR (500 MHz, $CDCl_3$, 25 °C): δ = 10.19 (s, 1H, *meso*), 10.15 (s, 2H, *meso*), 7.62 (s, 8H, Ar-*o*), 7.43 (s, 4H, Ar-*p*), 4.00–3.90 (m, 16H, ethyl), 1.89–1.82 (m, 24H, ethyl) ppm; ^{13}C NMR (126 MHz, $CDCl_3$, 25 °C): δ = 161.8 (q, J = 50 Hz, Ar-*ipso*), 153.9, 151.9, 150.2, 148.6, 148.1, 147.5, 145.7, 142.6, 134.9 (s, Ar-*o*), 128.9 (q, J = 32 Hz, Ar-*m*), 124.6 (q, J = 273 Hz, CF_3), 117.5 (t, J = 3.9 Hz, Ar-*p*), 111.3, 109.0, 19.8, 19.7, 19.5, 19.3, 18.6, 18.5, 18.3, 17.9 ppm; ^{19}F NMR (471 MHz, $CDCl_3$, 25 °C): δ = –62.4 (24F) ppm; UV/Vis (CH_2Cl_2): $\lambda_{\max}$ (ε [M^{-1} cm^{-1}]) = 312 (3.2×10^{4}), 359 (3.5×10^{4}), 405 (9.9×10^{4}), 531 (5.2×10^{3}), 568 (5.9×10^{3}), 661 (4.5×10^{4}) nm; FL (λ_{ex} = 550 nm, CH_2Cl_2): $\lambda_{\max}$ (nm) = 675 (<1%); HRMS (APCI-TOF, positive mode): [thiaporphyrinium]$^{+}$ Calcd for $C_{35}H_{43}N_4SZn$ 615.2494; Found 615.2495; HRMS (APCI-TOF, negative mode): [$BAr^{F}{}_4$]$^{-}$ Calcd for $C_{32}H_{12}{}^{11}BF_{24}$ 863.0649; Found 863.0668.

NMR Spectra

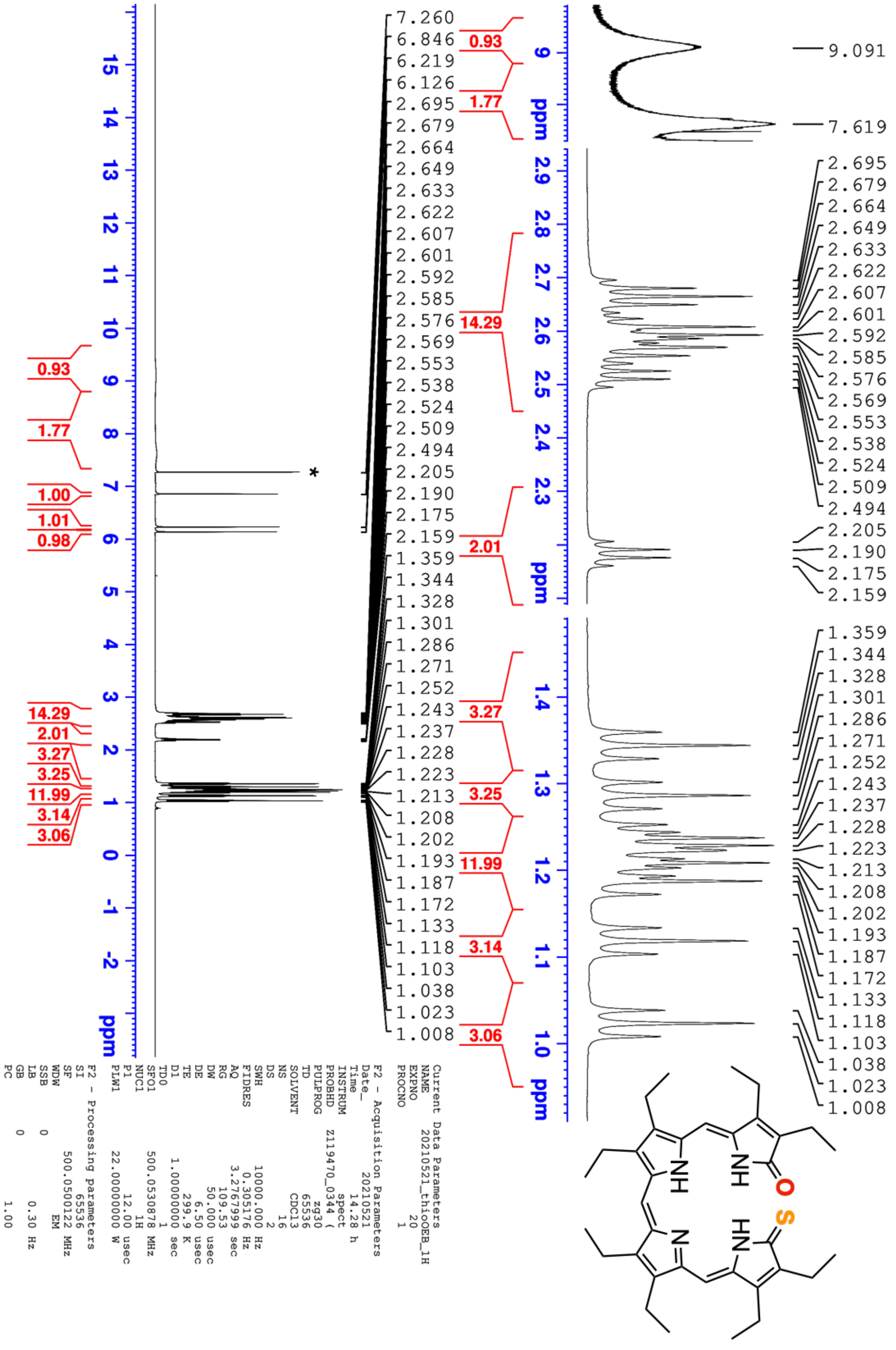

```
Current Data Parameters
NAME        20210521_thioOEB_1H
EXPNO                        20
PROCNO                        1

F2 - Acquisition Parameters
Date_                  20210521
Time                    14.28 h
INSTRUM                   spect
PROBHD       Z119470_0344 (
PULPROG                    zg30
TD                        65536
SOLVENT                   CDCl3
NS                           16
DS                            2
SWH                10000.000 Hz
FIDRES              0.305176 Hz
AQ                3.2767999 sec
RG                       109.53
DW                   50.000 usec
DE                     6.50 usec
TE                      299.9 K
D1               1.00000000 sec
TD0                           1
SFO1            500.0530878 MHz
NUC1                         1H
P1                    12.00 usec
PLW1            22.00000000 W

F2 - Processing parameters
SI                        65536
SF              500.0500122 MHz
WDW                          EM
SSB                           0
LB                      0.30 Hz
GB                            0
PC                         1.00
```

Figure S1. ^{1}H NMR (500 MHz) spectrum of **2** in $CDCl_3$ at 25 °C.

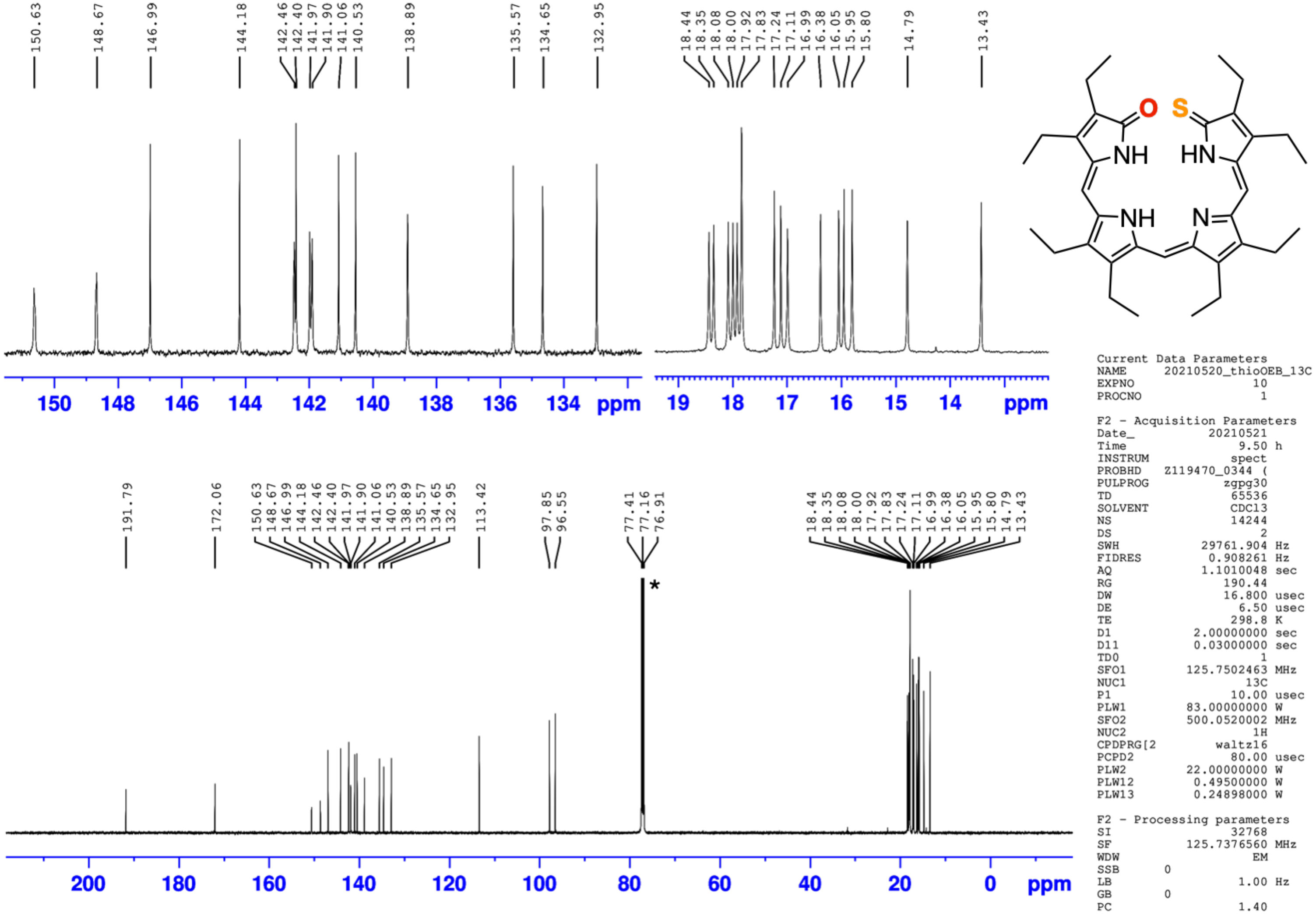

```
Current Data Parameters
NAME      20210520_thioOEB_13C
EXPNO                       10
PROCNO                       1

F2 - Acquisition Parameters
Date_               20210521
Time                    9.50 h
INSTRUM                spect
PROBHD   Z119470_0344 (
PULPROG              zgpg30
TD                     65536
SOLVENT                CDCl3
NS                     14244
DS                         2
SWH                29761.904 Hz
FIDRES              0.908261 Hz
AQ                 1.1010048 sec
RG                    190.44
DW                    16.800 usec
DE                      6.50 usec
TE                     298.8 K
D1                2.00000000 sec
D11               0.03000000 sec
TD0                        1
SFO1             125.7502463 MHz
NUC1                     13C
P1                     10.00 usec
PLW1             83.00000000 W
SFO2             500.0520002 MHz
NUC2                      1H
CPDPRG[2             waltz16
PCPD2                  80.00 usec
PLW2             22.00000000 W
PLW12             0.49500000 W
PLW13             0.24898000 W

F2 - Processing parameters
SI                     32768
SF               125.7376560 MHz
WDW                       EM
SSB      0
LB                      1.00 Hz
GB       0
PC                      1.40
```

Figure S2. ^{13}C NMR (126 MHz) spectrum of **2** in $CDCl_3$ at 25 °C.

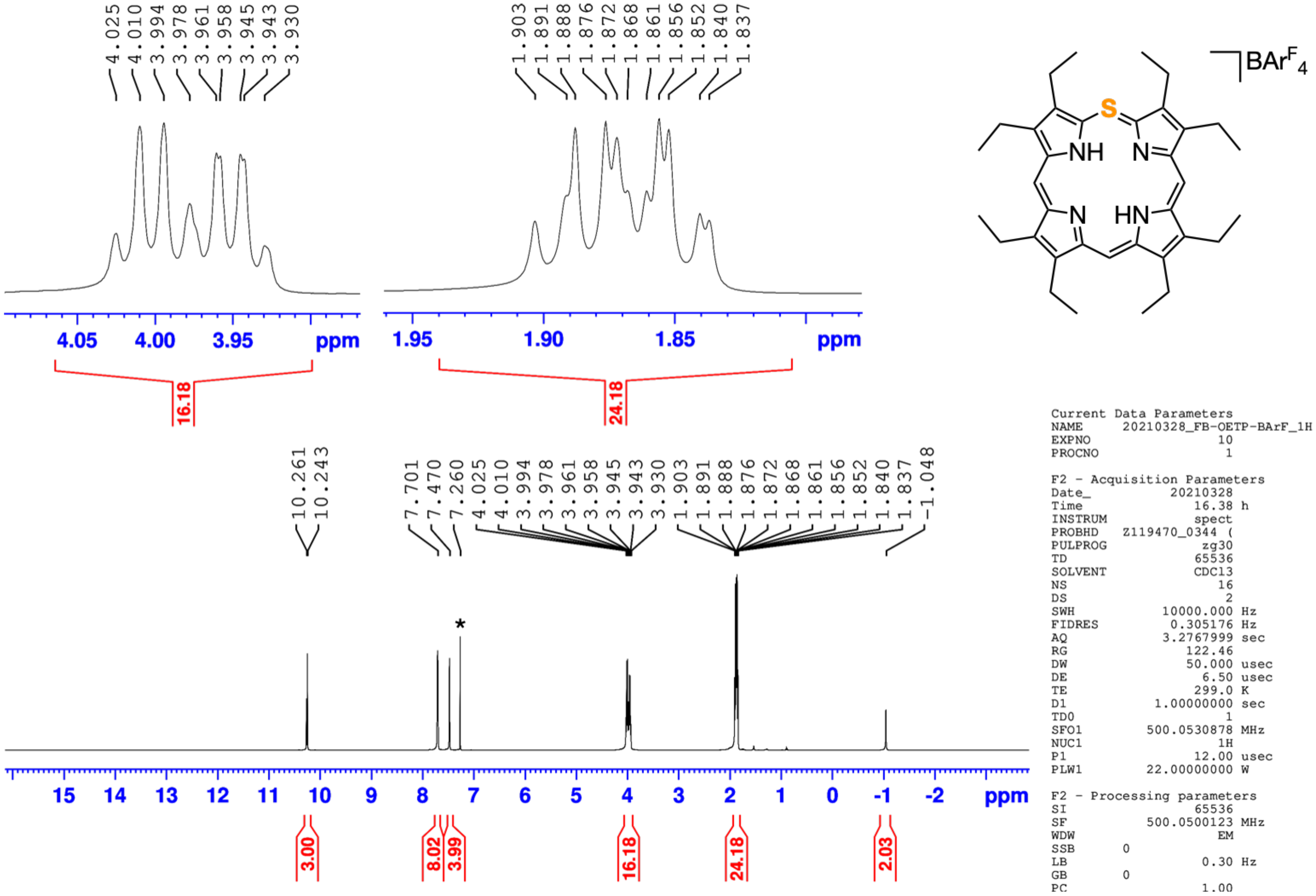

```
Current Data Parameters
NAME      20210328_FB-OETP-BArF_1H
EXPNO                    10
PROCNO                    1

F2 - Acquisition Parameters
Date_              20210328
Time                  16.38 h
INSTRUM               spect
PROBHD     Z119470_0344 (
PULPROG                zg30
TD                    65536
SOLVENT               CDCl3
NS                       16
DS                        2
SWH               10000.000 Hz
FIDRES             0.305176 Hz
AQ                3.2767999 sec
RG                   122.46
DW                   50.000 usec
DE                     6.50 usec
TE                    299.0 K
D1               1.00000000 sec
TD0                       1
SFO1            500.0530878 MHz
NUC1                     1H
P1                    12.00 usec
PLW1            22.00000000 W

F2 - Processing parameters
SI                    65536
SF              500.0500123 MHz
WDW                      EM
SSB      0
LB                     0.30 Hz
GB       0
PC                     1.00
```

Figure S3. ^{1}H NMR (500 MHz) spectrum of **3-2H** in $CDCl_3$ at 25 °C.

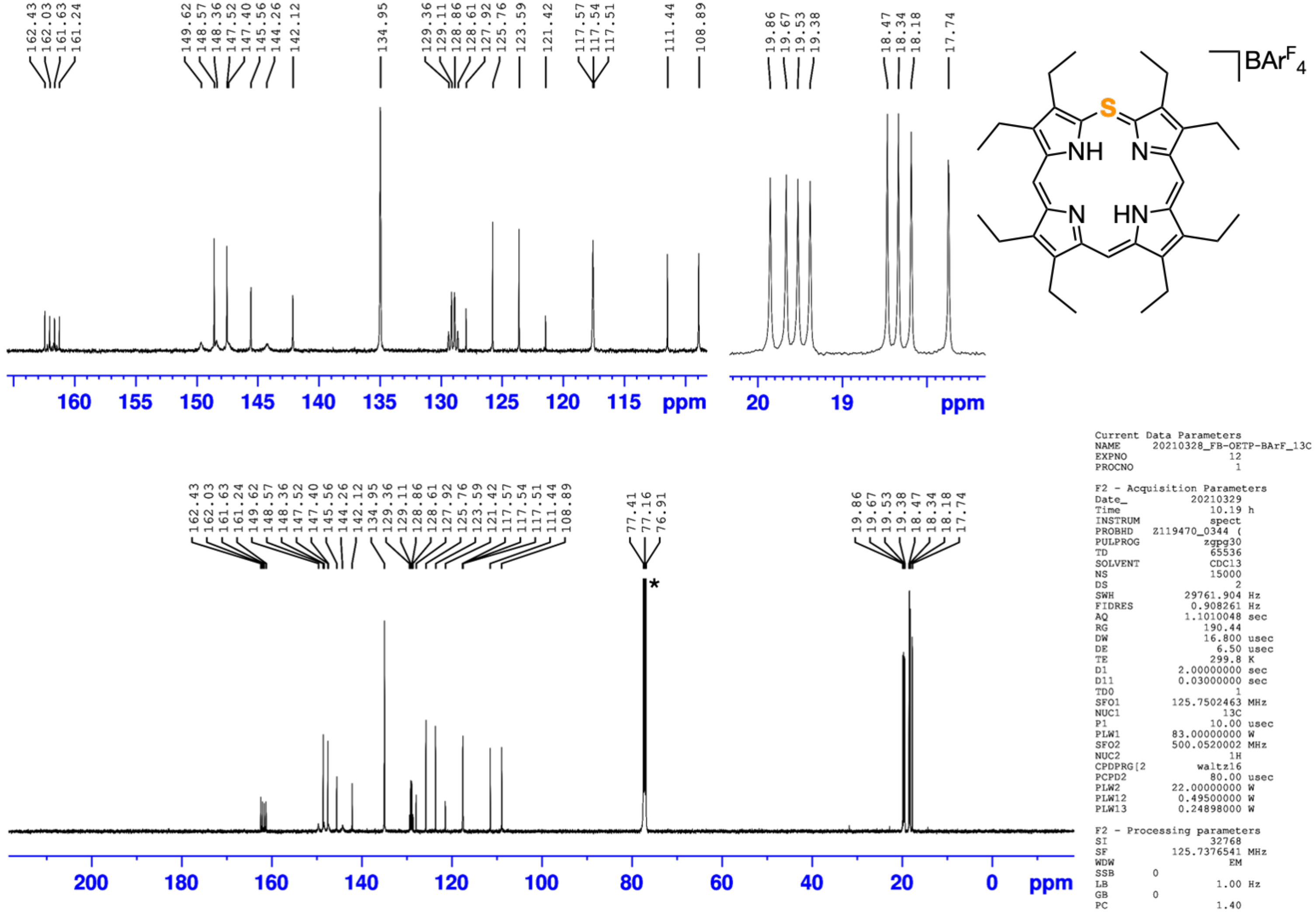

```
Current Data Parameters
NAME       20210328_FB-OETP-BArF_13C
EXPNO                        12
PROCNO                        1

F2 - Acquisition Parameters
Date_               20210329
Time                   10.19 h
INSTRUM                spect
PROBHD     Z119470_0344 (
PULPROG              zgpg30
TD                    65536
SOLVENT               CDCl3
NS                    15000
DS                        2
SWH               29761.904 Hz
FIDRES             0.908261 Hz
AQ                1.1010048 sec
RG                   190.44
DW                   16.800 usec
DE                     6.50 usec
TE                    299.8 K
D1               2.00000000 sec
D11              0.03000000 sec
TD0                       1
SFO1            125.7502463 MHz
NUC1                    13C
P1                    10.00 usec
PLW1            83.00000000 W
SFO2            500.0520002 MHz
NUC2                     1H
CPDPRG[2            waltz16
PCPD2                 80.00 usec
PLW2            22.00000000 W
PLW12            0.49500000 W
PLW13            0.24898000 W

F2 - Processing parameters
SI                    32768
SF              125.7376541 MHz
WDW                      EM
SSB        0
LB                     1.00 Hz
GB         0
PC                     1.40
```

Figure S4. ^{13}C NMR (126 MHz) spectrum of **3-2H** in $CDCl_3$ at 25 °C.

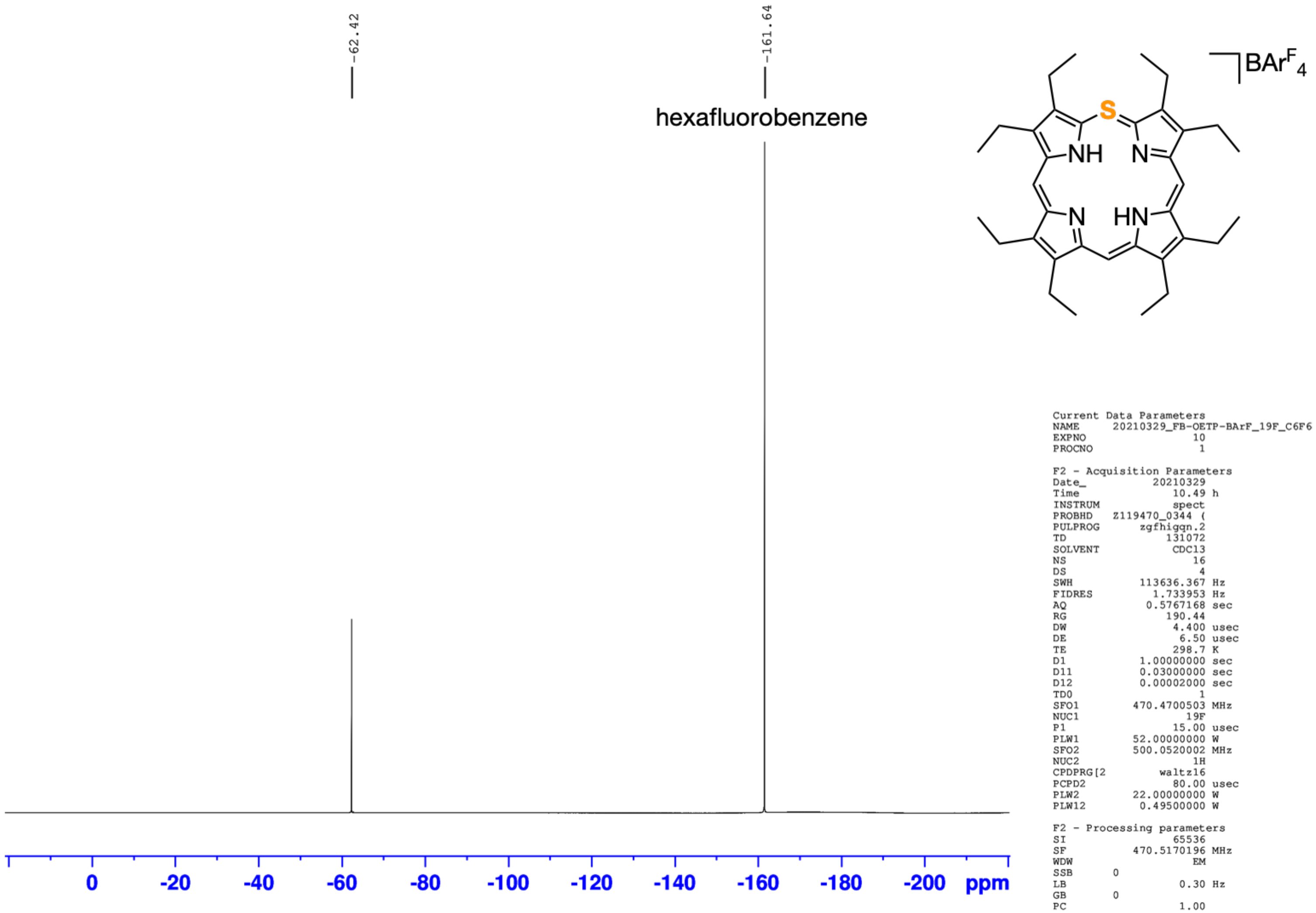

```
Current Data Parameters
NAME     20210329_FB-OETP-BArF_19F_C6F6
EXPNO                 10
PROCNO                 1

F2 - Acquisition Parameters
Date_           20210329
Time               10.49 h
INSTRUM            spect
PROBHD   Z119470_0344 (
PULPROG       zgfhigqn.2
TD                131072
SOLVENT            CDCl3
NS                    16
DS                     4
SWH           113636.367 Hz
FIDRES          1.733953 Hz
AQ             0.5767168 sec
RG                190.44
DW                 4.400 usec
DE                  6.50 usec
TE                 298.7 K
D1            1.00000000 sec
D11           0.03000000 sec
D12           0.00002000 sec
TD0                    1
SFO1         470.4700503 MHz
NUC1                 19F
P1                 15.00 usec
PLW1         52.00000000 W
SFO2         500.0520002 MHz
NUC2                  1H
CPDPRG[2         waltz16
PCPD2              80.00 usec
PLW2         22.00000000 W
PLW12         0.49500000 W

F2 - Processing parameters
SI                 65536
SF           470.5170196 MHz
WDW                   EM
SSB       0
LB                  0.30 Hz
GB        0
PC                  1.00
```

Figure S5. ^{19}F NMR (471 MHz) spectrum of **3-2H** in $CDCl_3$ at 25 °C.

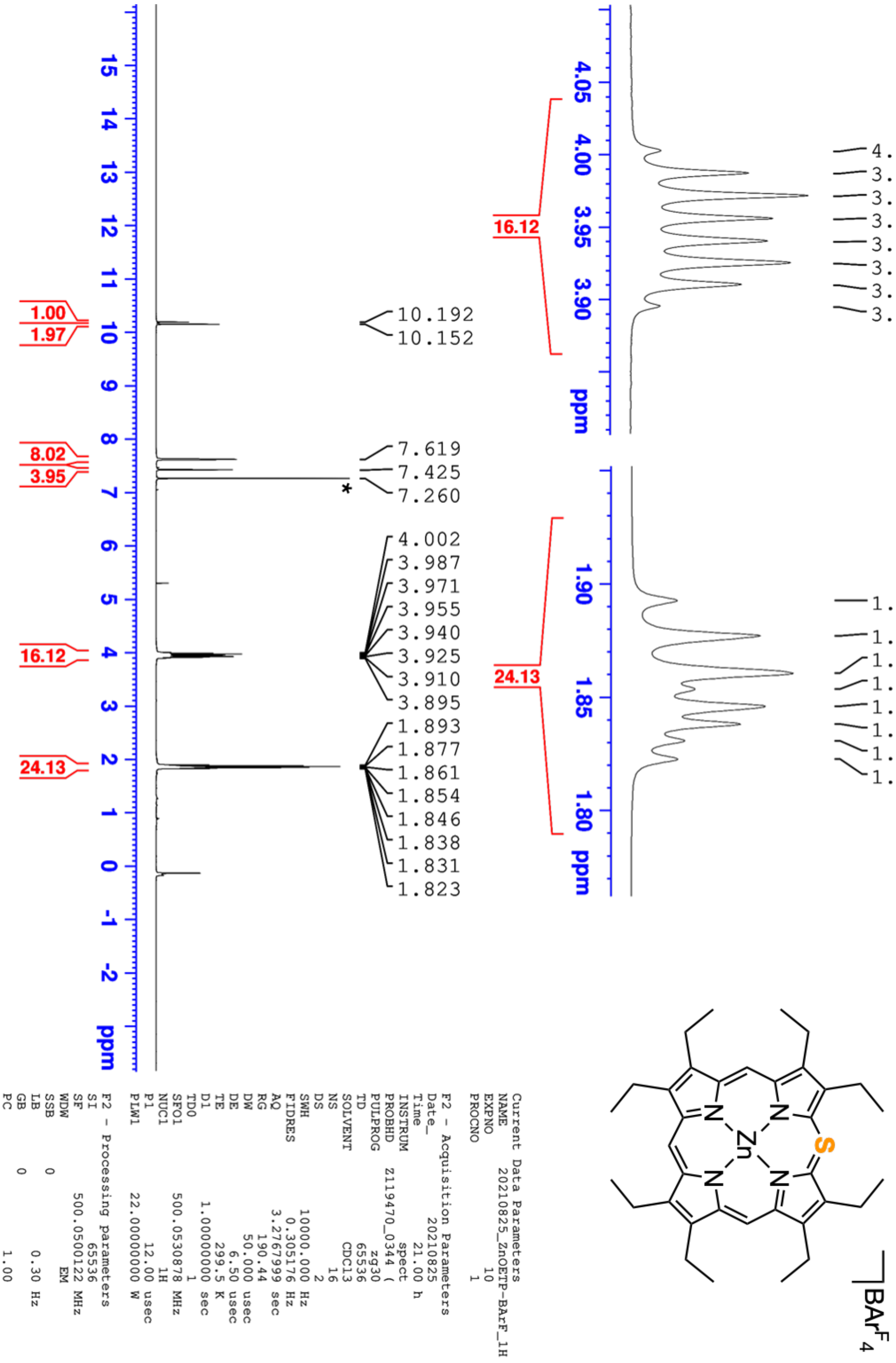

```
Current Data Parameters
NAME      20210825_ZnOETP-BArF_1H
EXPNO                   10
PROCNO                   1

F2 - Acquisition Parameters
Date_             20210825
Time              21.00 h
INSTRUM              spect
PROBHD    Z119470_0344 (
PULPROG               zg30
TD                   65536
SOLVENT              CDCl3
NS                      16
DS                       2
SWH              10000.000 Hz
FIDRES            0.305176 Hz
AQ               3.2767999 sec
RG                  190.44
DW                  50.000 usec
DE                    6.50 usec
TE                   299.5 K
D1              1.00000000 sec
TD0                      1
SFO1           500.0530878 MHz
NUC1                    1H
P1                   12.00 usec
PLW1           22.00000000 W

F2 - Processing parameters
SI                   65536
SF             500.0500122 MHz
WDW                     EM
SSB      0
LB                    0.30 Hz
GB       0
PC                    1.00
```

Figure S6. ^{1}H NMR (500 MHz) spectrum of **3-Zn** in $CDCl_3$ at 25 °C.

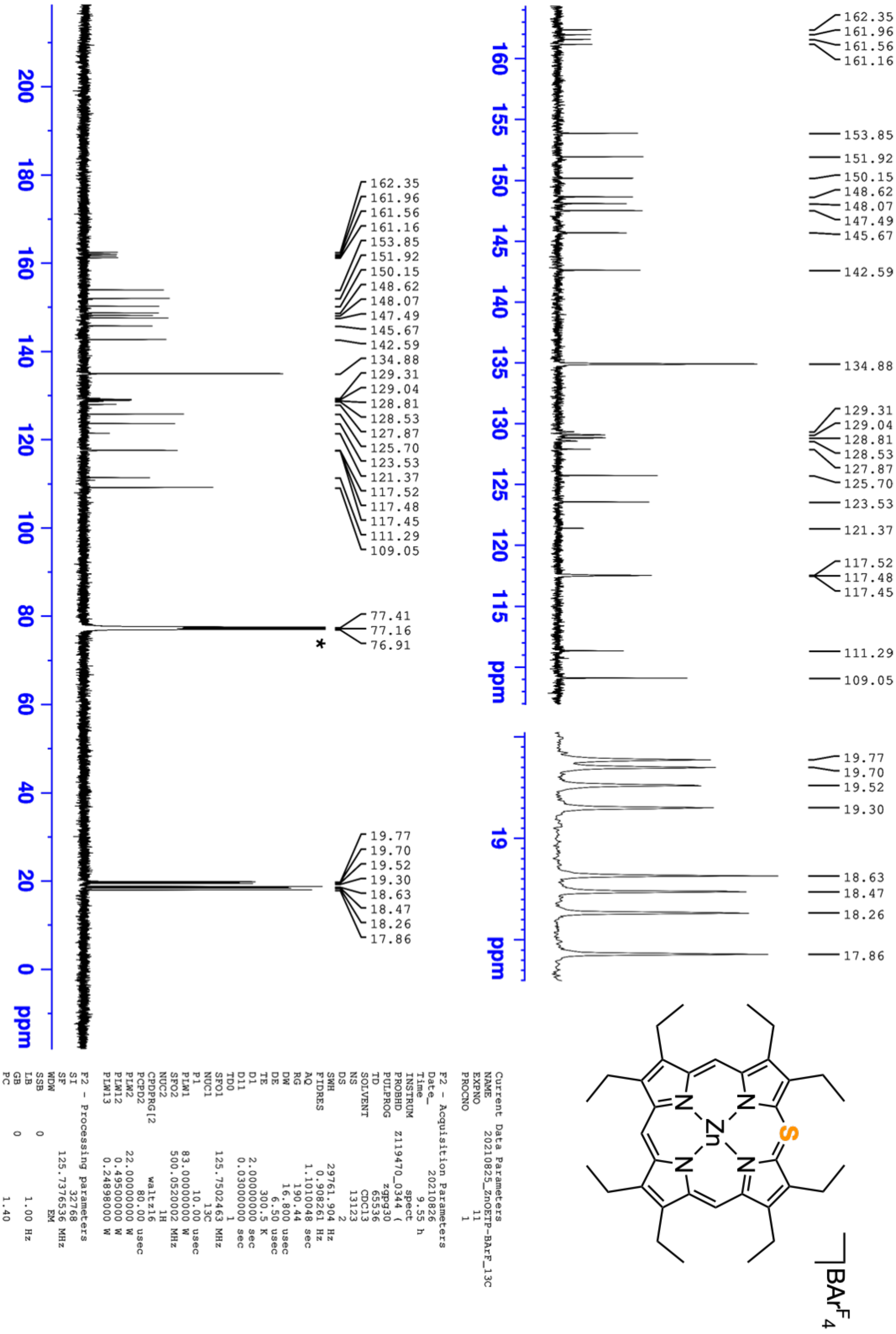

Figure S7. ^{13}C NMR (126 MHz) spectrum of **3-Zn** in $CDCl_3$ at 25 °C.

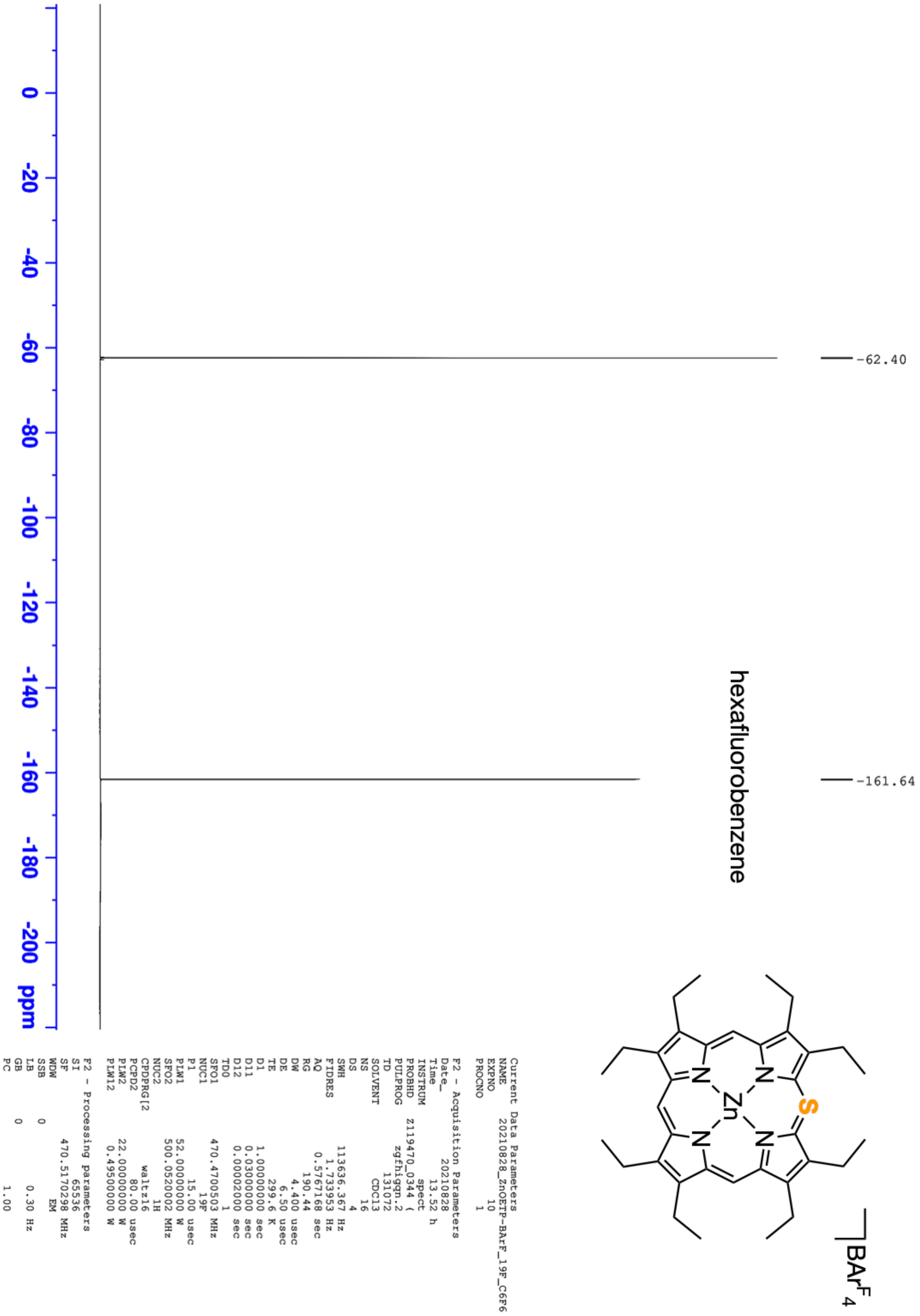

```
Current Data Parameters
NAME     20210828_ZnOETP-BArF_19F_C6F6
EXPNO                10
PROCNO                1

F2 - Acquisition Parameters
Date_          20210828
Time              13.52 h
INSTRUM           spect
PROBHD   Z119470_0344 (
PULPROG     zgfhigqn.2
TD               131072
SOLVENT           CDCl3
NS                   16
DS                    4
SWH          113636.367 Hz
FIDRES         1.733953 Hz
AQ            0.5767168 sec
RG               190.44
DW                4.400 usec
DE                 6.50 usec
TE                299.6 K
D1           1.00000000 sec
D11          0.03000000 sec
D12          0.00002000 sec
TD0                   1
SFO1        470.4700503 MHz
NUC1                19F
P1                15.00 usec
PLW1        52.00000000 W
SFO2        500.0520002 MHz
NUC2                 1H
CPDPRG[2        waltz16
PCPD2             80.00 usec
PLW2        22.00000000 W
PLW12        0.49500000 W

F2 - Processing parameters
SI                65536
SF          470.5170298 MHz
WDW                  EM
SSB                   0
LB                 0.30 Hz
GB                    0
PC                 1.00
```

Figure S8. ^{19}F NMR (471 MHz) spectrum of **3-Zn** in $CDCl_3$ at 25 °C.

3. High-Resolution Mass Spectra

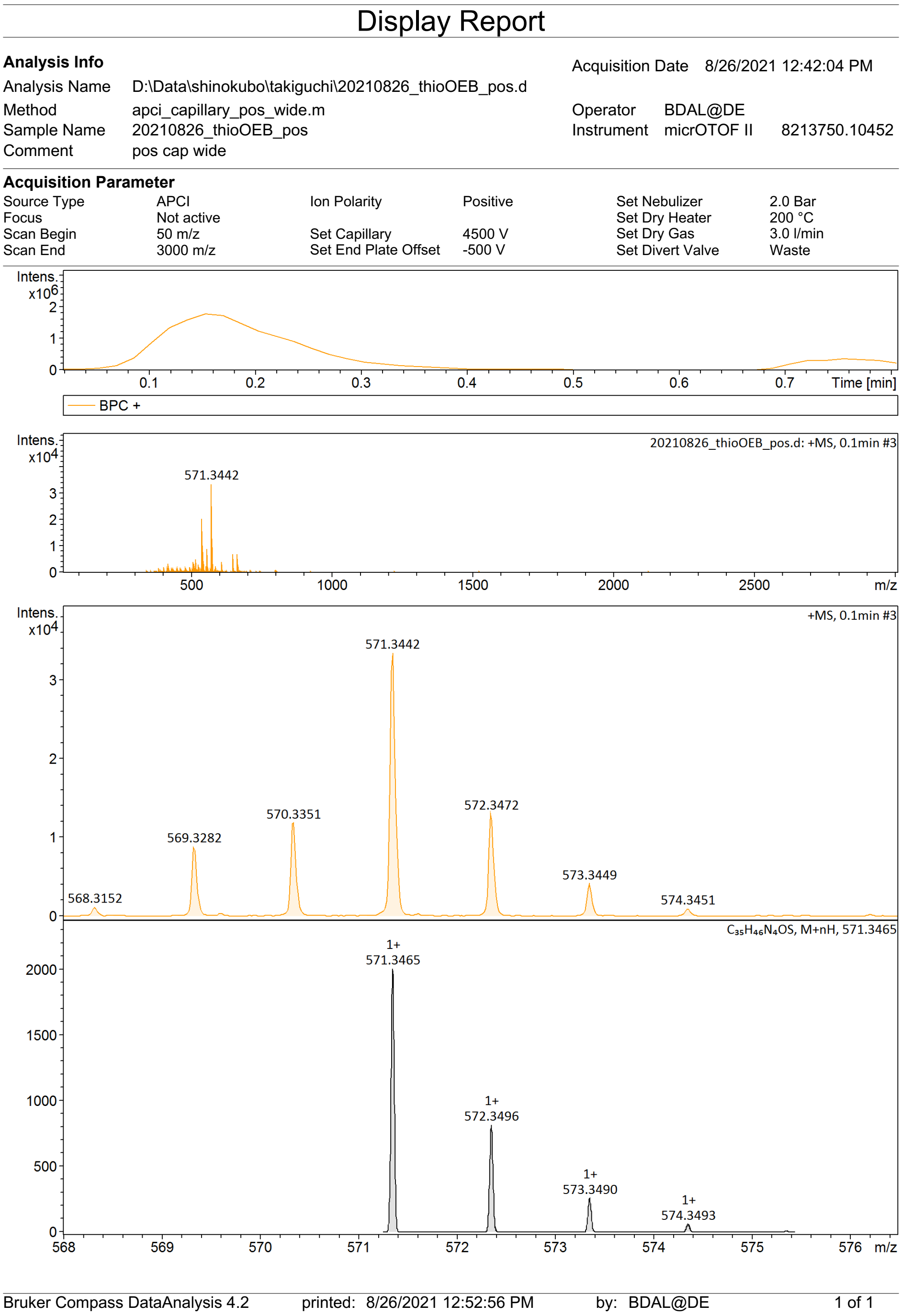

Display Report

Analysis Info

Analysis Name	D:\Data\shinokubo\takiguchi\20210826_thioOEB_pos.d	Acquisition Date	8/26/2021 12:42:04 PM
Method	apci_capillary_pos_wide.m	Operator	BDAL@DE
Sample Name	20210826_thioOEB_pos	Instrument	micrOTOF II 8213750.10452
Comment	pos cap wide		

Acquisition Parameter

Source Type	APCI	Ion Polarity	Positive	Set Nebulizer	2.0 Bar
Focus	Not active			Set Dry Heater	200 °C
Scan Begin	50 m/z	Set Capillary	4500 V	Set Dry Gas	3.0 l/min
Scan End	3000 m/z	Set End Plate Offset	-500 V	Set Divert Valve	Waste

Bruker Compass DataAnalysis 4.2 printed: 8/26/2021 12:52:56 PM by: BDAL@DE 1 of 1

Figure S9. APCI-TOF-MS (positive mode) spectrum of **2**.

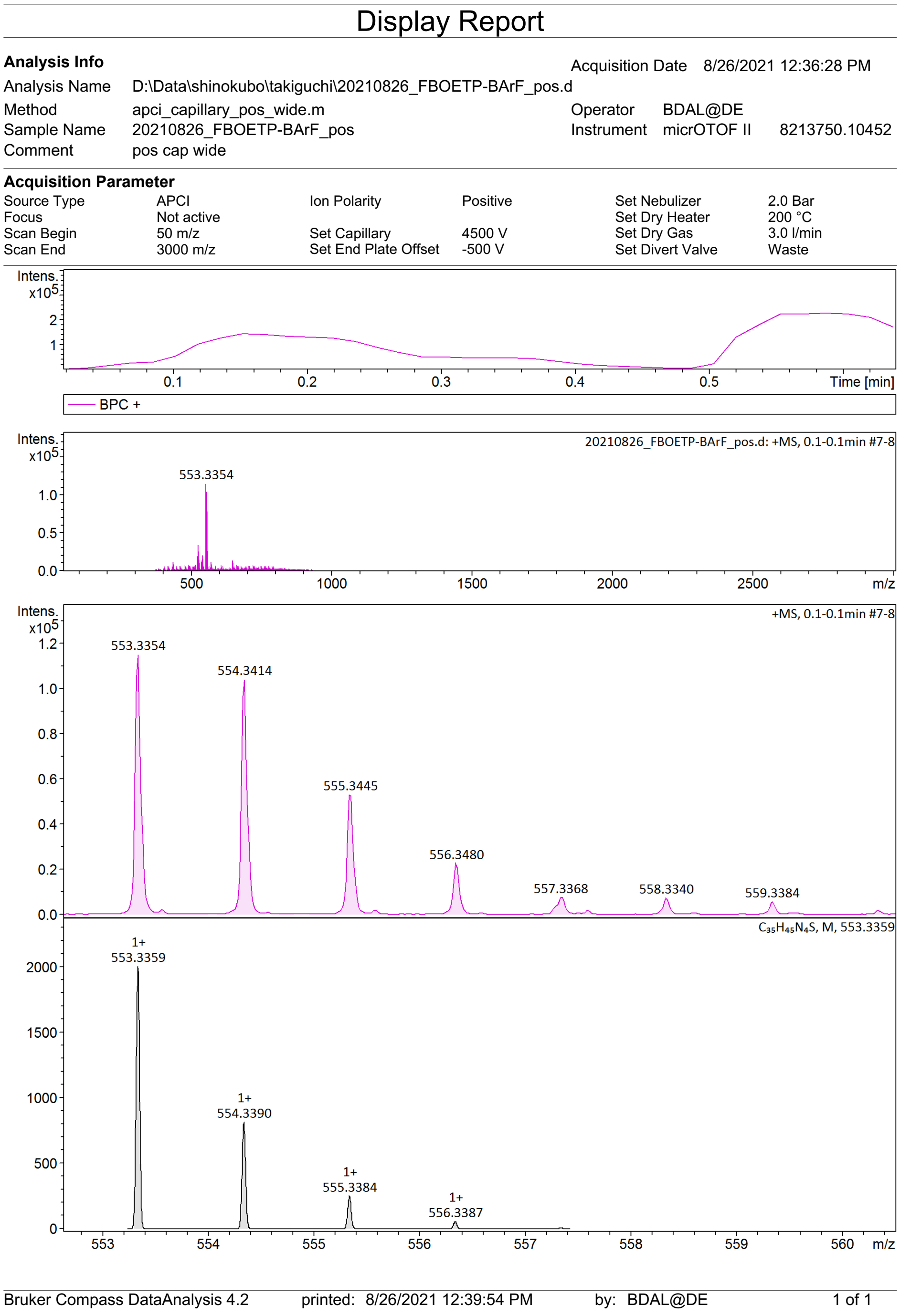

Display Report

Analysis Info

Analysis Name D:\Data\shinokubo\takiguchi\20210826_FBOETP-BArF_pos.d
Method apci_capillary_pos_wide.m
Sample Name 20210826_FBOETP-BArF_pos
Comment pos cap wide

Acquisition Date 8/26/2021 12:36:28 PM
Operator BDAL@DE
Instrument micrOTOF II 8213750.10452

Acquisition Parameter

Source Type	APCI	Ion Polarity	Positive	Set Nebulizer	2.0 Bar
Focus	Not active			Set Dry Heater	200 °C
Scan Begin	50 m/z	Set Capillary	4500 V	Set Dry Gas	3.0 l/min
Scan End	3000 m/z	Set End Plate Offset	-500 V	Set Divert Valve	Waste

Bruker Compass DataAnalysis 4.2 printed: 8/26/2021 12:39:54 PM by: BDAL@DE 1 of 1

Figure S10. APCI-TOF-MS (positive mode) spectrum of **3-2H**.

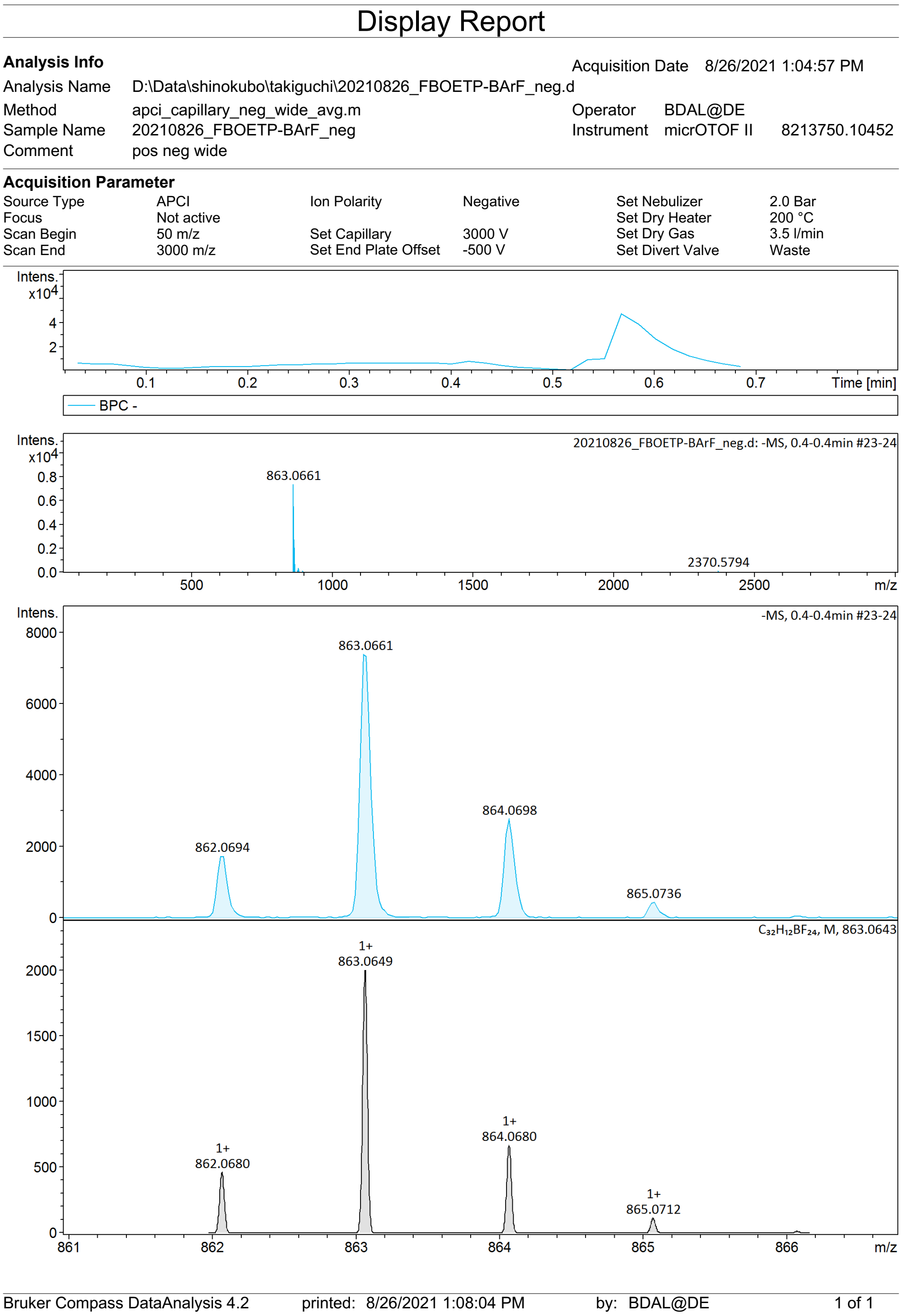

Display Report

Analysis Info

Analysis Name D:\Data\shinokubo\takiguchi\20210826_FBOETP-BArF_neg.d
Method apci_capillary_neg_wide_avg.m
Sample Name 20210826_FBOETP-BArF_neg
Comment pos neg wide

Acquisition Date 8/26/2021 1:04:57 PM
Operator BDAL@DE
Instrument micrOTOF II 8213750.10452

Acquisition Parameter

Source Type	APCI	Ion Polarity	Negative	Set Nebulizer	2.0 Bar
Focus	Not active			Set Dry Heater	200 °C
Scan Begin	50 m/z	Set Capillary	3000 V	Set Dry Gas	3.5 l/min
Scan End	3000 m/z	Set End Plate Offset	-500 V	Set Divert Valve	Waste

Bruker Compass DataAnalysis 4.2 printed: 8/26/2021 1:08:04 PM by: BDAL@DE 1 of 1

Figure S11. APCI-TOF-MS (negative mode) spectrum of **3-2H**.

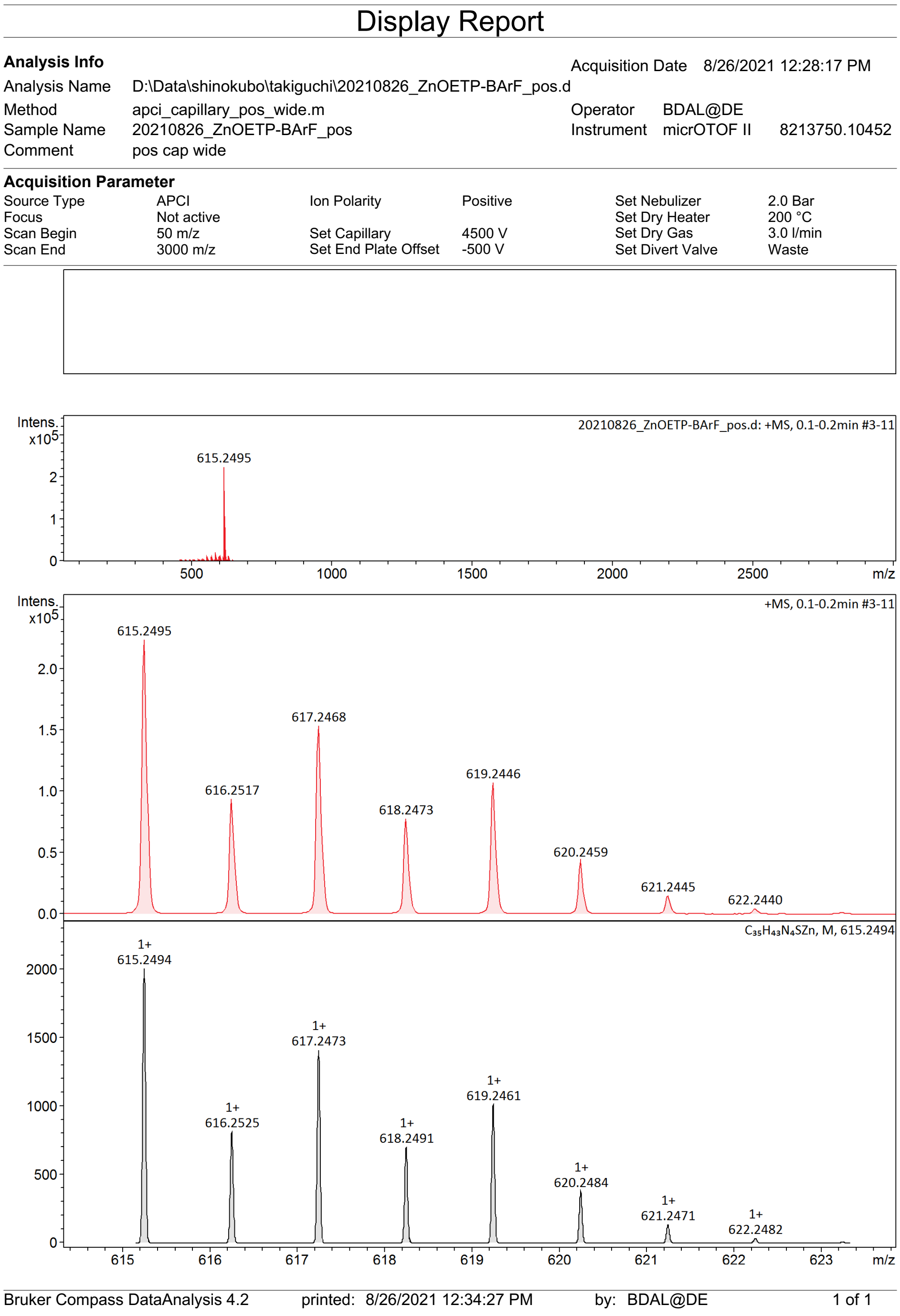

Display Report

Analysis Info

Acquisition Date 8/26/2021 12:28:17 PM

Analysis Name D:\Data\shinokubo\takiguchi\20210826_ZnOETP-BArF_pos.d

Method apci_capillary_pos_wide.m

Operator BDAL@DE

Sample Name 20210826_ZnOETP-BArF_pos

Instrument micrOTOF II 8213750.10452

Comment pos cap wide

Acquisition Parameter

Source Type	APCI	Ion Polarity	Positive	Set Nebulizer	2.0 Bar
Focus	Not active			Set Dry Heater	200 °C
Scan Begin	50 m/z	Set Capillary	4500 V	Set Dry Gas	3.0 l/min
Scan End	3000 m/z	Set End Plate Offset	-500 V	Set Divert Valve	Waste

Bruker Compass DataAnalysis 4.2 printed: 8/26/2021 12:34:27 PM by: BDAL@DE 1 of 1

Figure S12. APCI-TOF-MS (positive mode) spectrum of **3-Zn**.

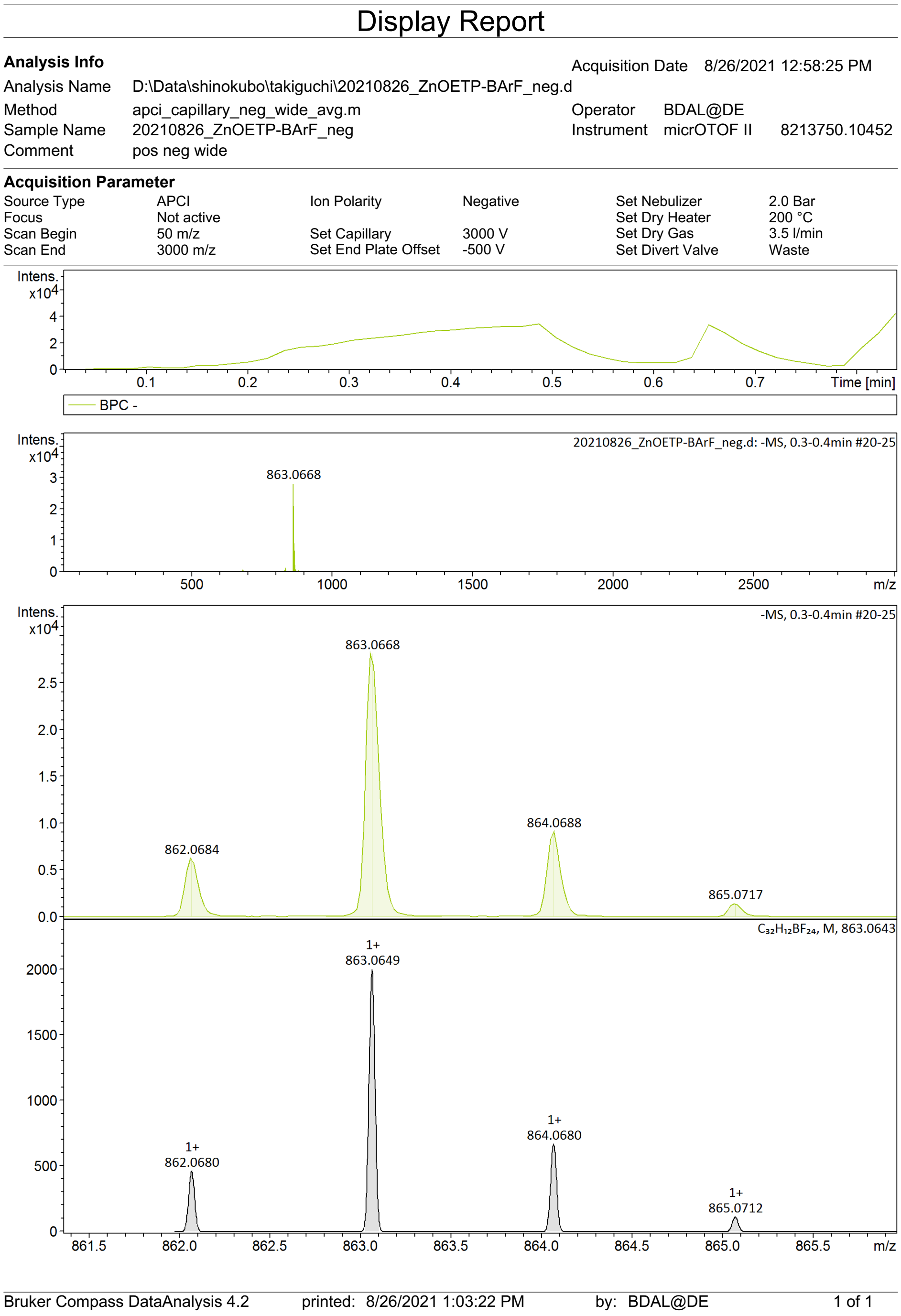

Display Report

Analysis Info

Analysis Name	D:\Data\shinokubo\takiguchi\20210826_ZnOETP-BArF_neg.d	Acquisition Date	8/26/2021 12:58:25 PM
Method	apci_capillary_neg_wide_avg.m	Operator	BDAL@DE
Sample Name	20210826_ZnOETP-BArF_neg	Instrument	micrOTOF II 8213750.10452
Comment	pos neg wide		

Acquisition Parameter

Source Type	APCI	Ion Polarity	Negative	Set Nebulizer	2.0 Bar
Focus	Not active			Set Dry Heater	200 °C
Scan Begin	50 m/z	Set Capillary	3000 V	Set Dry Gas	3.5 l/min
Scan End	3000 m/z	Set End Plate Offset	-500 V	Set Divert Valve	Waste

Bruker Compass DataAnalysis 4.2 printed: 8/26/2021 1:03:22 PM by: BDAL@DE 1 of 1

Figure S13. APCI-TOF-MS (negative mode) spectrum of **3-Zn**.

4. Crystal Data

Table S1. Crystallographic data of **2**, **3-2H**, and **3-Zn**.

compound	**2**	**3-2H**
Formula	$C_{35}H_{46}N_4OS$	$C_{35}H_{45}N_4S^+$, $C_{32}H_{12}BF_{24}^-$, $0.5(C_6H_{12})$
Formula weight	570.82	1459.11
Crystal system	monoclinic	triclinic
Space group	$P2_1/n$ (No. 14)	P-1 (No. 2)
Crystal color	purple	purple
Crystal description	block	block
a [Å]	11.9883(5)	13.4974(6)
b [Å]	21.0001(7)	14.6725(7)
c [Å]	12.8601(5)	18.5690(9)
α [°]	90	107.949(2)
β [°]	103.3000(10)	99.555(2)
γ [°]	90	99.629(2)
V [Å^3]	3150.8(2)	3355.1(3)
Z	4	2
d_{calcd} [g cm^{-3}]	1.203	1.444
R_1 ($I > 2\sigma(I)$)	0.0655	0.0683
wR_2 (all data)	0.1270	0.1809
Goodness-of-fit	1.113	1.019
Temperature [K]	93(2)	93(2)
Solvent	chloroform/hexane	dichloroethane/cyclohexane
CCDC No.	2143344	2143345

Table S1 (continued)

compound	**3-Zn**
Formula	$C_{35}H_{43}N_4SZn^+$, $C_{32}H_{12}BF_{24}^-$, $1.5(C_6H_6)$
Formula weight	1597.55
Crystal system	triclinic
Space group	*P*-1 (No. 2)
Crystal color	purple
Crystal description	block
a [Å]	15.2381(2)
b [Å]	15.9224(3)
c [Å]	16.4963(3)
α [°]	80.9350(10)
β [°]	63.946(2)
γ [°]	89.9040(10)
V [Å^3]	3540.51(12)
Z	2
d_{calcd} [g cm^{-3}]	1.499
R_1 ($I > 2\sigma(I)$)	0.0473
wR_2 (all data)	0.1291
Goodness-of-fit	1.033
Temperature [K]	93(2)
Solvent	chloroform[a]/benzene
CCDC No.	2143346

[a] Amylene added chloroform was used to avoid axial coordination by ethanol added as a stabilizer.

5. Cyclic Voltammograms

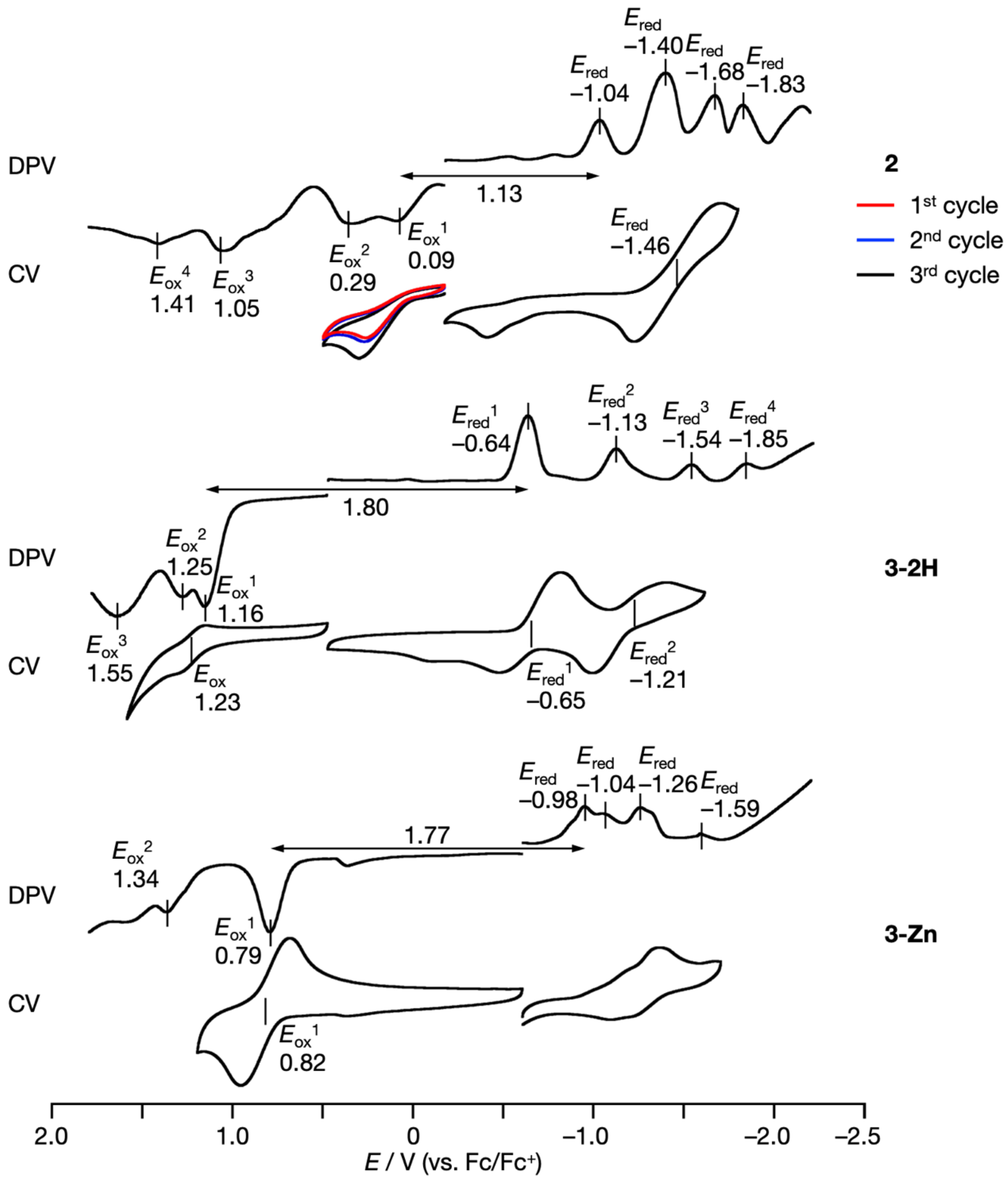

Figure S14. Cyclic voltammograms and differential pulse voltammograms of **2**, **3-2H**, and **3-Zn**.

6. DFT Calculations

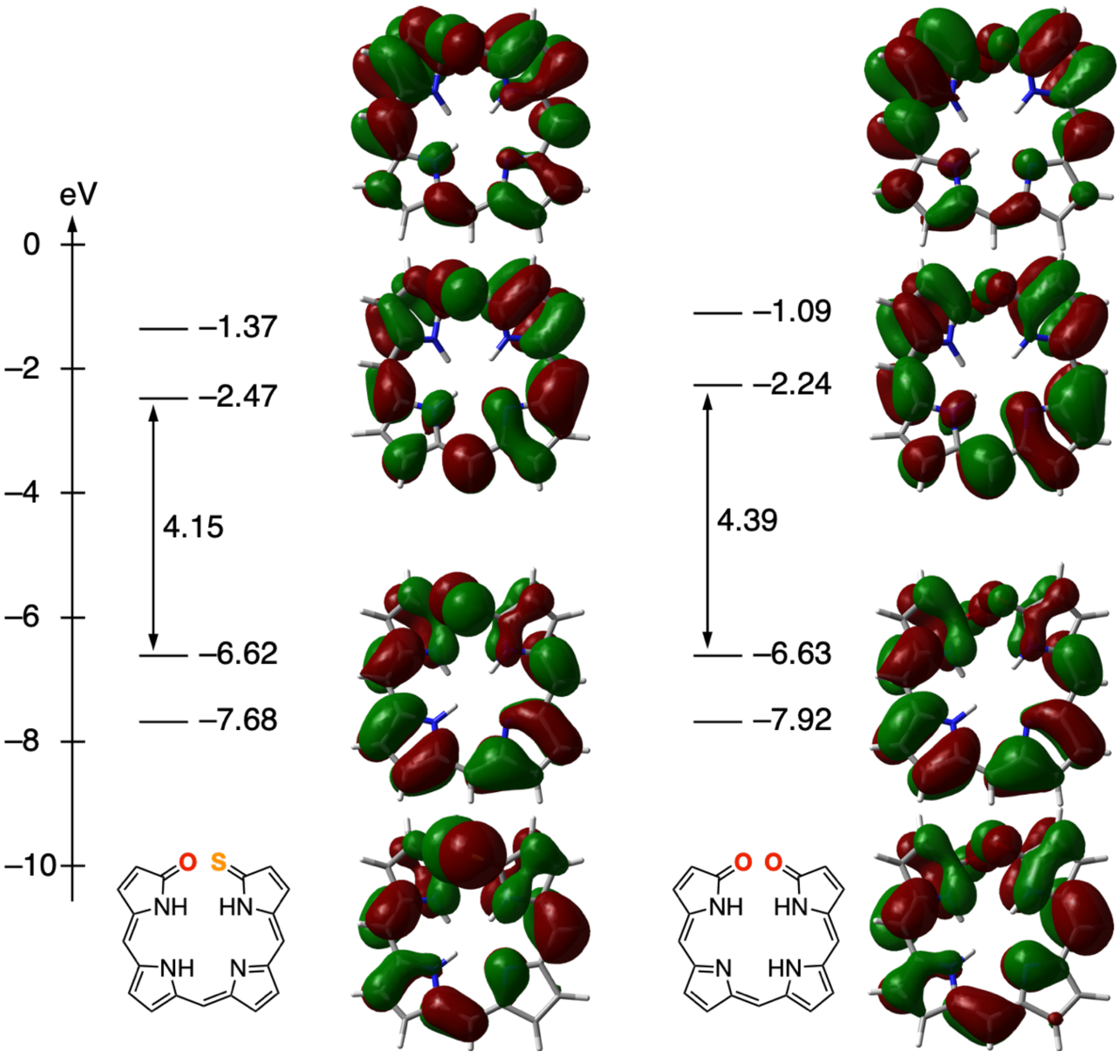

Figure S15. Kohn–Sham MOs and energy diagrams of **2** (left) and **4** (right).

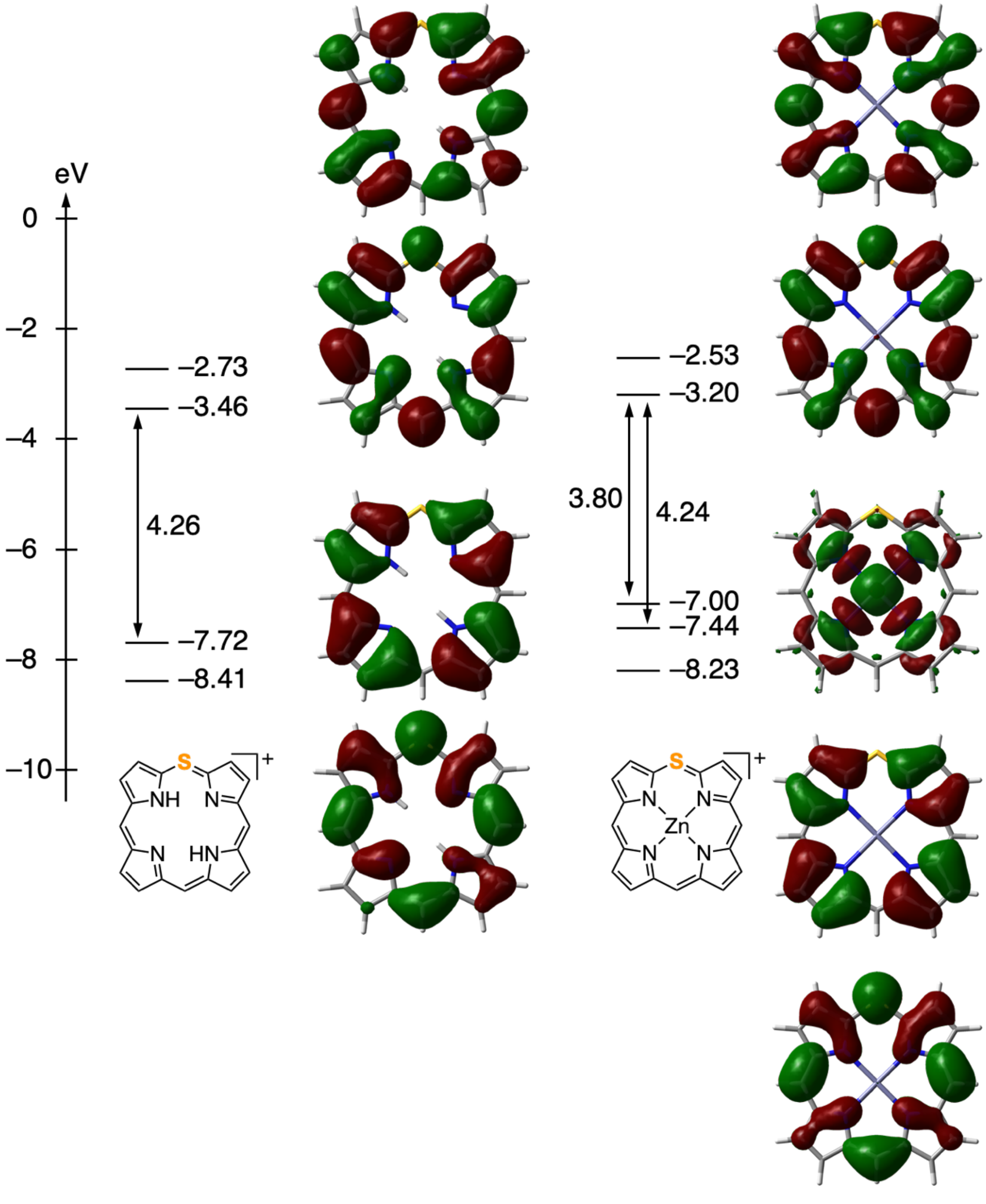

Figure S16. Kohn–Sham MOs and energy diagrams of **3-2H** (left) and **3-Zn** (right).

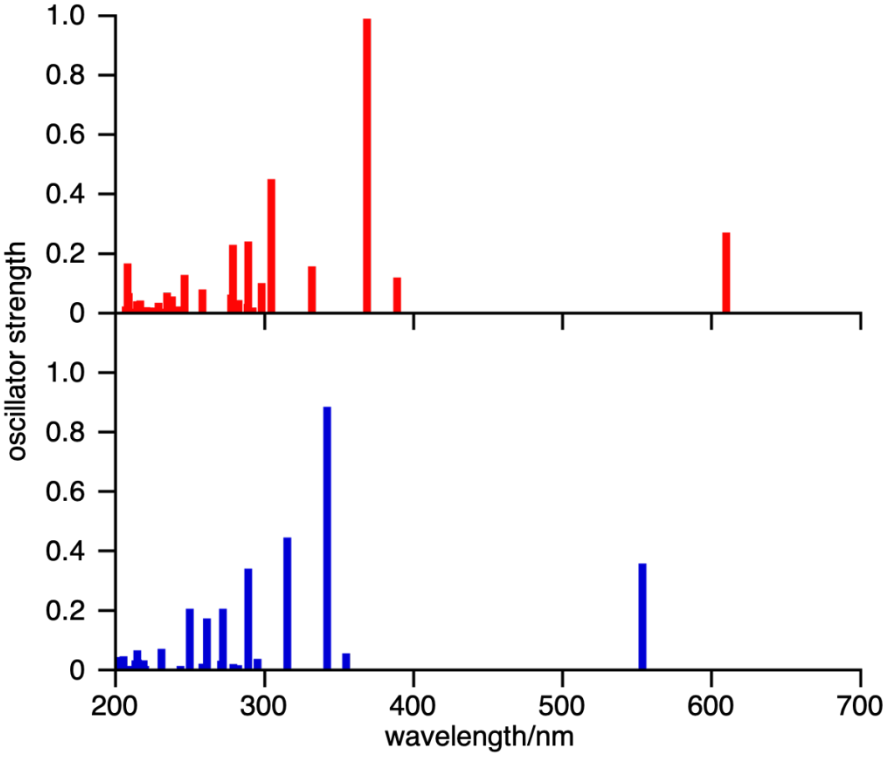

Figure S17. Simulated electronic absorption spectra of **2** (top) and **4** (bottom).

Table S2. Summary of simulated maximal absorption wavelength.

compound	wavelength/nm	oscillator strength	transition
2	609.71	0.2584	HOMO–1 → LUMO+1 (2.1%)
			HOMO → LUMO (97.9%)
4	553.64	0.3459	HOMO → LUMO (100%)

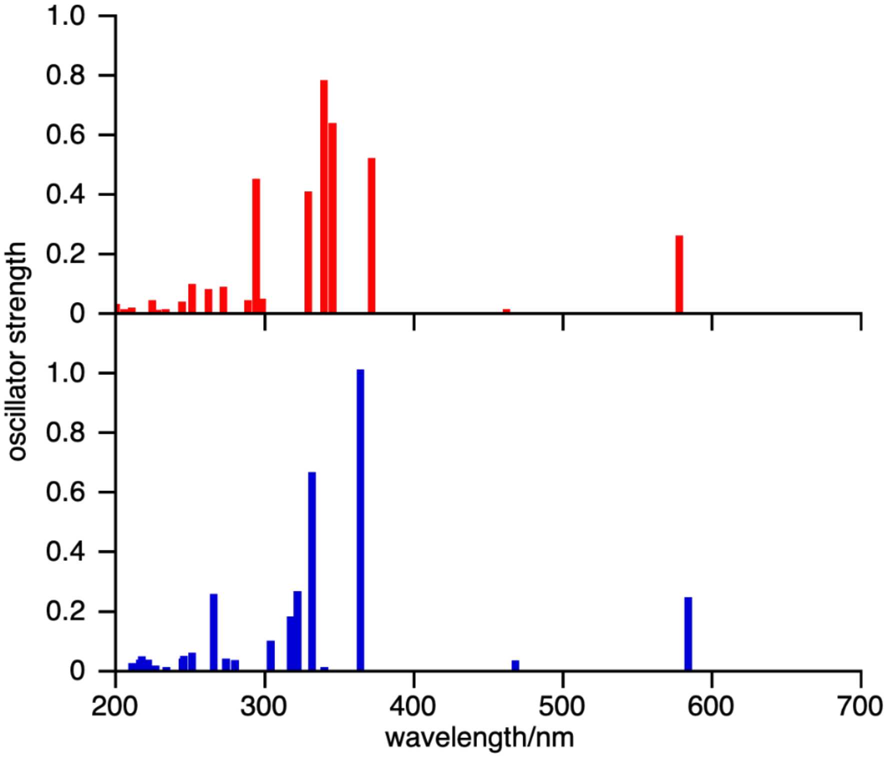

Figure S18. Simulated electronic absorption spectra of **3-2H** (top) and **3-Zn** (bottom).

Table S3. Summary of simulated excited states of **3-2H**.

wavelength/nm	oscillator strength	transition
577.94	0.2487	HOMO–1 → LUMO+1 (12.5%)
		HOMO → LUMO (87.5%)
462.00	0.0035	HOMO–1 → LUMO (47.2%)
		HOMO → LUMO+1 (52.8%)

Table S4. Summary of simulated excited states of **3-Zn**.

wavelength/nm	oscillator strength	transition
1175.82	0.0000	HOMO → LUMO (100%)
731.96	0.0000	HOMO → LUMO+1 (100%)
584.08	0.2357	HOMO–2 → LUMO+1 (11.2%)
		HOMO–1 → LUMO (88.8%)
467.98	0.0229	HOMO–2 → LUMO (37.4%)
		HOMO–1 → LUMO+1 (62.6%)

Table S5. Relative free energies of the tautomers of porphyrin and porphyrin analogues (kcal mol^{-1}).

X	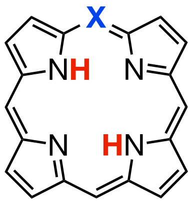 form A	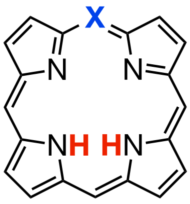 form B	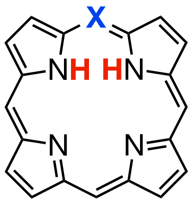 form C	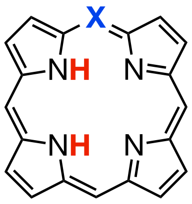 form D
S^+	0	+2.32	+15.31	+6.08
O^+ [a]	0	−1.49	+16.87	+5.81
CH[a]	0	+6.91	+6.91	+6.91

[a] The values are cited from ref. 5.

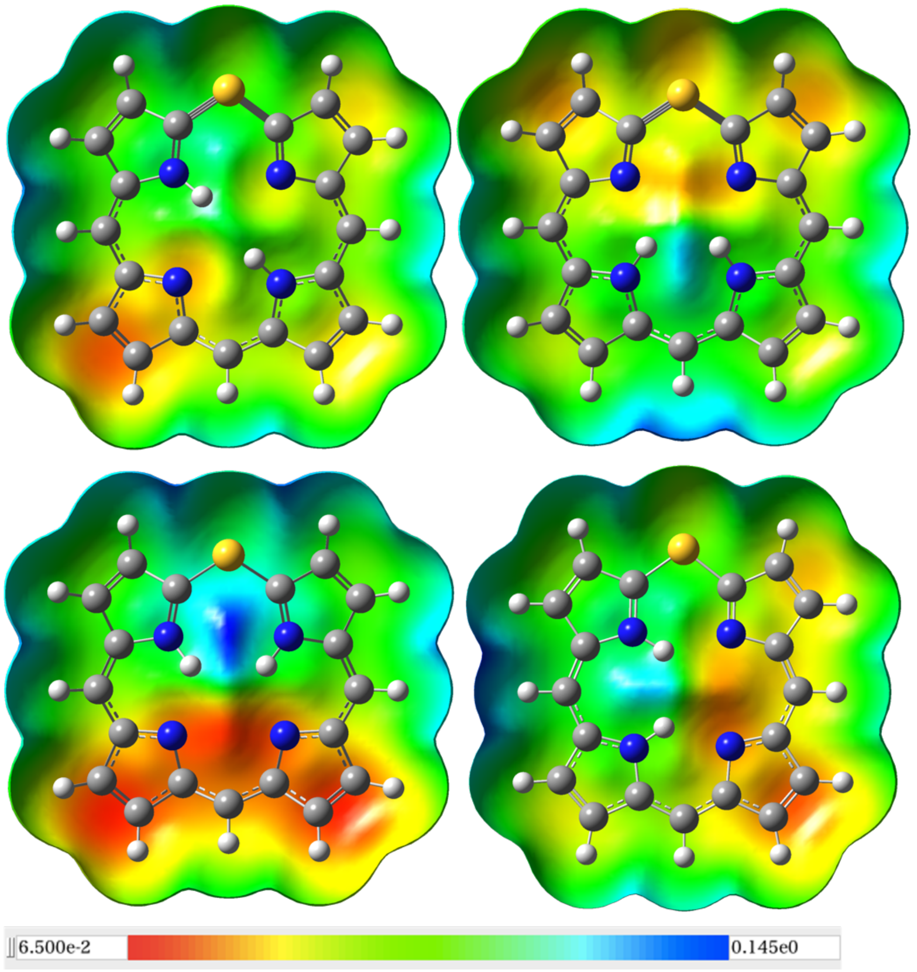

Figure S19. Electrostatic potential maps of isomers of **3-2H**.

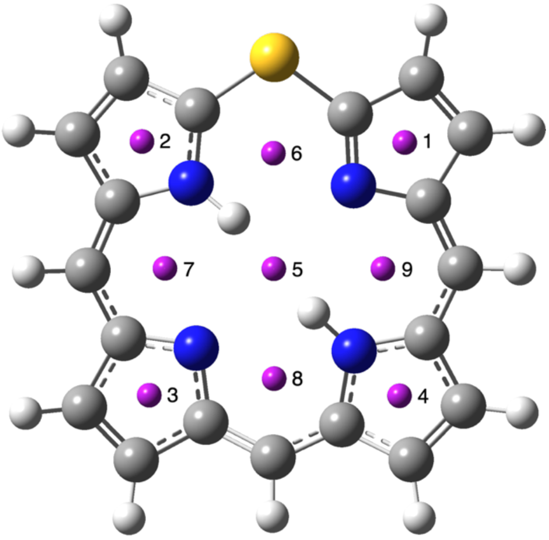

Table S6. Summary of NICS values of **3-2H**.

position	NICS(0)/NICS(1) (ppm)	position	NICS(0)/NICS(1) (ppm)
1	–1.96/–5.85	6	–13.07/–11.92
2	–10.13/–10.61	7	–11.61/–12.08
3	–1.56/–5.62	8	–11.31/–11.91
4	–10.21/–10.78	9	–11.77/–12.10
5	–10.03/–9.46		

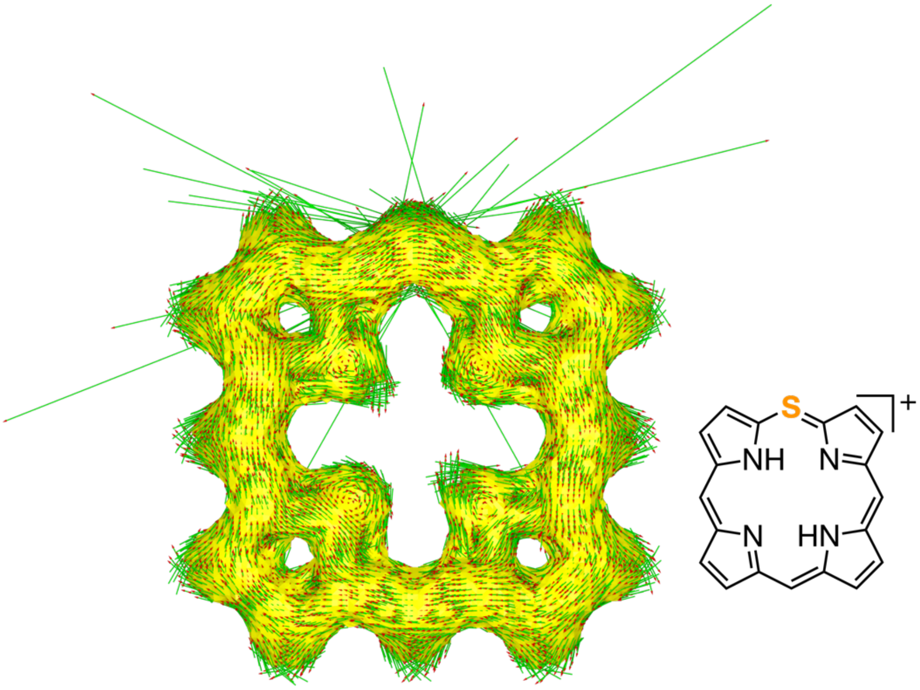

Figure S20. ACID plot of **3-2H**.

Cartesian Coordinates of **2**

E_{total} = –1424.394570 Hartree

C	-2.41261935	-1.99780182	0.33743414
C	-2.66649737	-3.40675691	0.16250769
C	-1.46632490	-3.98605032	-0.06662026
C	-0.48484473	-2.92628503	0.01209996
N	-1.04951379	-1.75183580	0.24264847
C	-3.35783606	-1.02780664	0.52400406
C	-3.13788595	0.36359745	0.54662551
C	-4.02348075	1.40215873	0.84102276
N	-1.92664125	0.93968348	0.25307613
C	-3.31808917	2.59623501	0.74837612
C	-2.00867143	2.28955514	0.36810154
C	-0.93025659	3.20341593	0.11133223
C	0.93505565	-3.13124670	-0.10242428
C	0.16675696	2.99223912	-0.63471096
C	1.26406746	3.93518344	-0.82270656
N	0.50327662	1.86931391	-1.38458614
C	2.16735359	3.40453337	-1.65017442
C	1.68544625	2.07489433	-2.07490114
C	1.88605806	-2.26019001	0.28569176
C	3.32885204	-2.40599193	0.21269340
N	1.66882588	-1.03115666	0.88907034
C	3.89135939	-1.31445384	0.75250215
C	2.83100082	-0.41968129	1.21157653
H	-0.13893954	1.14665398	-1.66902994
O	2.17432293	1.29528671	-2.86885820
H	-1.10646286	0.36155438	0.11345120
H	0.74349542	-0.68748935	1.10039669
H	-1.03196311	4.18643192	0.55222435
H	-4.38495282	-1.34780857	0.65237748
H	1.26789465	-4.08182040	-0.49866197
H	3.09867633	3.82781002	-1.99012534
H	1.30153510	4.89399656	-0.32828994
H	-3.69622637	3.59321198	0.90665159
H	-5.06364307	1.27559954	1.09591805
H	-3.63854584	-3.87513512	0.19253621
H	-1.25202484	-5.02736179	-0.25209358
H	3.82438382	-3.26363789	-0.21528016
H	4.93906111	-1.08911728	0.86437933
S	2.98028535	1.03615680	1.98896600

Cartesian Coordinates of **4**

E_{total} = –1101.419439 Hartree

C	-2.42567034	-1.99359043	0.35063726
C	-2.67713198	-3.40903294	0.21126221
C	-1.47805586	-3.99106798	-0.00245500
C	-0.49526357	-2.92625442	0.04414800
N	-1.05824092	-1.74862822	0.24640758
C	-3.37459502	-1.02970470	0.51577595
C	-3.16710205	0.36839457	0.52526770
C	-4.06750246	1.39862104	0.79103675
N	-1.95694805	0.95131600	0.24776822
C	-3.37162396	2.60081151	0.69604105
C	-2.05403453	2.30391635	0.34579836
C	-0.97923573	3.22705108	0.10804604
C	0.92417846	-3.14511715	-0.08204526
C	0.15071589	3.01837334	-0.58716657
C	1.24733080	3.96707490	-0.73631047
N	0.53537571	1.88301213	-1.29669164
C	2.19907901	3.42804336	-1.50263685
C	1.74968361	2.08798995	-1.92941608
C	1.88508685	-2.26579683	0.24734755
C	3.33121900	-2.46097823	0.15456109
N	1.70578684	-1.00406494	0.77879094
C	3.94579085	-1.37172168	0.61904375
C	2.91264005	-0.40032646	1.05472490
H	-0.09117467	1.16010306	-1.61412818
O	3.05850420	0.69653345	1.55808331
O	2.28378250	1.30087058	-2.68644991
H	-1.13025855	0.37893792	0.12617138
H	0.79657642	-0.62990471	1.00195105
H	-1.11135928	4.21673650	0.52555707
H	-4.40066363	-1.35527664	0.63818354
H	1.24310137	-4.11642072	-0.43698446
H	3.14412464	3.85300849	-1.79997308
H	1.25183246	4.93521898	-0.25880722
H	-3.76286206	3.59552007	0.83624089
H	-5.11078304	1.26439225	1.02862825
H	-3.64887862	-3.87708278	0.25505740
H	-1.26123679	-5.03634592	-0.16111824
H	3.78041606	-3.36036704	-0.23832687
H	5.00319749	-1.17621426	0.69693165

Cartesian Coordinates of **3-2H** (form A)

E_{total} = –1348.369489 Hartree

C	-1.23579022	-2.80004599	-0.00001509
C	-2.50694215	-3.48957678	-0.00002311
C	-3.45232930	-2.52843265	-0.00003107
C	-2.73916317	-1.26935489	-0.00001934
N	-1.41127492	-1.44813744	-0.00000499
C	-0.00882770	-3.44022368	-0.00000613
C	1.24498949	-2.84590570	0.00000630
C	2.50978833	-3.48414110	0.00002054
N	1.47183109	-1.49893319	0.00000479
C	3.46639748	-2.50490953	0.00002192
C	2.79960097	-1.25573499	0.00001608
C	3.40911812	0.01431006	0.00001657
C	-3.39000528	-0.02338867	-0.00001892
C	2.82569573	1.24322869	0.00001319
C	3.58706461	2.47823674	0.00001768
N	1.45900336	1.52081349	0.00001239
C	2.69667172	3.48252558	0.00000962
C	1.39943003	2.82818422	0.00000901
C	-2.85045029	1.23142308	-0.00001084
C	-3.57645978	2.45775875	-0.00000628
N	-1.50519075	1.57006251	-0.00000398
C	-2.68529206	3.48429909	-0.00000432
C	-1.39094528	2.89951267	-0.00000059
H	4.49144051	-0.00150911	0.00002011
H	-4.47257868	-0.05380602	-0.00002458
H	-0.01972552	-4.52278335	-0.00000653
H	4.53728637	-2.62821906	0.00003001
H	2.65967646	-4.55177807	0.00002659
H	-2.63680417	-4.56072985	-0.00002810
H	-4.52555234	-2.63993288	-0.00004233
H	-4.65257207	2.52501083	-0.00000809
H	-2.88558568	4.54303701	-0.00000314
H	4.66399065	2.54167217	0.00002184
H	2.87168326	4.54670966	0.00000704
S	0.01706425	3.86247316	0.00000450
H	-0.72540937	0.92191524	-0.00000218
H	0.73369045	-0.80678164	-0.00000414

Cartesian Coordinates of **3-2H** (form B)

E_{total} = –1348.365796 Hartree

C	-1.26149196	-2.70959865	-0.00001368
C	-2.48217960	-3.43485925	-0.00001677
C	-3.51242214	-2.53520725	-0.00002199
C	-2.93951855	-1.24344861	-0.00002290
N	-1.59668138	-1.37796979	-0.00001977
C	0.00000223	-3.27847983	-0.00000346
C	1.26149560	-2.70959690	0.00000776
C	2.48218425	-3.43485583	0.00000872
N	1.59668321	-1.37796756	0.00001636
C	3.51242554	-2.53520242	0.00001618
C	2.93952019	-1.24344454	0.00001990
C	3.60007997	0.00887608	0.00002340
C	-3.60007998	0.00887115	-0.00002347
C	2.98690225	1.21932090	0.00001995
C	3.65955505	2.50862179	0.00002041
N	1.60278573	1.39967269	0.00001429
C	2.69542935	3.43902573	0.00001485
C	1.43626405	2.69120917	0.00001101
C	-2.98690391	1.21931678	-0.00001727
C	-3.65955847	2.50861674	-0.00001437
N	-1.60278761	1.39967046	-0.00001153
C	-2.69543402	3.43902201	-0.00000687
C	-1.43626776	2.69120714	-0.00000528
H	4.68150057	-0.01732492	0.00002688
H	-4.68150054	-0.01733126	-0.00002683
H	0.00000299	-4.36119119	-0.00000459
H	4.57007167	-2.74136807	0.00001760
H	2.54766963	-4.51117493	0.00000304
H	-2.54766349	-4.51117844	-0.00001358
H	-4.57006799	-2.74137433	-0.00002387
H	-4.72833470	2.65529477	-0.00001687
H	-2.79076491	4.51334681	-0.00000217
H	4.72833108	2.65530134	0.00002388
H	2.79075875	4.51335066	0.00001280
S	-0.00000230	3.64880331	0.00000373
H	-1.01407526	-0.54382258	-0.00002189
H	1.01407594	-0.54382115	0.00002014

Cartesian Coordinates of **3-2H** (form C)

E_{total} = –1348.345096 Hartree

C	-1.26627997	-2.63352580	-0.00002445
C	-2.47984260	-3.43181384	-0.00002914
C	-3.50887384	-2.56181600	-0.00003969
C	-2.90737382	-1.24628244	-0.00004429
N	-1.56168985	-1.31486762	-0.00003702
C	0.00000218	-3.20887299	-0.00000353
C	1.26628352	-2.63352405	0.00001851
C	2.47984723	-3.43181043	0.00002148
N	1.56169161	-1.31486545	0.00003375
C	3.50887729	-2.56181119	0.00003368
C	2.90737548	-1.24627844	0.00004108
C	3.60937309	-0.03677080	0.00004106
C	-3.60937304	-0.03677577	-0.00004153
C	3.03500625	1.21154365	0.00003685
C	3.65663671	2.48471607	-0.00000314
N	1.66688616	1.42602104	0.00005667
C	2.67383322	3.43052831	-0.00001745
C	1.43231083	2.74184702	0.00001802
C	-3.03500787	1.21153945	-0.00003425
C	-3.65664006	2.48471102	0.00000900
N	-1.66688807	1.42601865	-0.00005368
C	-2.67383783	3.43052458	0.00002553
C	-1.43231451	2.74184496	-0.00001178
H	4.69107709	-0.07564145	0.00003051
H	-4.69107698	-0.07564787	-0.00003115
H	0.00000292	-4.29323336	-0.00000458
H	4.56723957	-2.77070334	0.00003512
H	2.51469249	-4.51031445	0.00001061
H	-2.51468638	-4.51031791	-0.00002041
H	-4.56723586	-2.77070953	-0.00004165
H	-4.72186907	2.65019704	0.00003341
H	-2.78451363	4.50258084	0.00006291
H	4.72186549	2.65020354	-0.00002681
H	2.78450753	4.50258471	-0.00005219
S	-0.00000250	3.67709636	0.00000412
H	-1.05146553	0.60882982	-0.00009598
H	1.05146466	0.60883143	0.00009679

Cartesian Coordinates of **3-2H** (form D)

E_{total} = –1348.359804 Hartree

C	-1.24638874	-2.93797993	-0.00001151
C	-2.53202739	-3.51708616	-0.00001909
C	-3.43893420	-2.48770353	-0.00002297
C	-2.71740246	-1.26932530	-0.00001692
N	-1.39085874	-1.59219276	-0.00000919
C	0.01608885	-3.57393541	-0.00000491
C	1.20997776	-2.91682180	0.00000240
C	2.52993461	-3.52454494	0.00000989
N	1.31892209	-1.53814907	0.00000196
C	3.40518020	-2.50645849	0.00001522
C	2.61026290	-1.27992778	0.00001021
C	3.22174729	0.01015768	0.00001411
C	-3.29542882	-0.00131199	-0.00001778
C	2.68674899	1.25602284	0.00001256
C	3.51951758	2.45368012	0.00001807
N	1.34071329	1.62523931	0.00000599
C	2.69368849	3.50900057	0.00001626
C	1.35875724	2.93063108	0.00001014
C	-2.76598623	1.26653385	-0.00001185
C	-3.54838162	2.45383989	-0.00001586
N	-1.43744860	1.67492078	-0.00000155
C	-2.71135562	3.53027147	-0.00001017
C	-1.39775405	3.01140194	-0.00000203
H	4.30518703	-0.01466678	0.00001974
H	-4.37832644	-0.01743520	-0.00002473
H	0.01758061	-4.65612052	-0.00000604
H	4.48340416	-2.54939839	0.00002197
H	2.73006371	-4.58455360	0.00001147
H	-2.73480710	-4.57542465	-0.00002189
H	-4.51488376	-2.55848773	-0.00002919
H	-4.62658271	2.46549376	-0.00002300
H	-2.96872977	4.57646092	-0.00001172
H	4.59834565	2.45288341	0.00002293
H	2.93092144	4.56106293	0.00001932
S	0.00145710	4.00366577	0.00000656
H	-0.56243800	1.14257543	0.00000600
H	-0.54928004	-1.01225290	-0.00000261

Cartesian Coordinates of **3-Zn**

E_{total} = –2352.089003 Hartree

C	2.71674411	-1.39271318	-0.00783393
C	3.33714173	-2.68056717	-0.08971706
C	2.33517366	-3.58737365	-0.21681657
C	1.11331301	-2.84318897	-0.21181413
N	1.35896972	-1.52475304	-0.08652113
C	3.39202649	-0.19155906	0.13406392
C	2.84106219	1.07617199	0.22619616
C	3.59317057	2.28606629	0.36486043
N	1.50384963	1.36010300	0.19679230
C	2.69287282	3.30031776	0.41682487
C	1.39938142	2.69900640	0.31039995
C	0.18717827	3.41392131	0.32199388
C	-0.16889920	-3.41207098	-0.31992396
C	-1.07570519	2.91348312	0.22391498
C	-2.27357372	3.71054236	0.23869854
N	-1.41669430	1.56962054	0.08976684
C	-3.31660322	2.86496342	0.11394068
C	-2.73679104	1.55076034	0.02400819
C	-1.36918559	-2.76774865	-0.31573454
C	-2.64420024	-3.42316215	-0.43139126
N	-1.56493007	-1.39259251	-0.19963414
C	-3.59147265	-2.46439968	-0.38587094
C	-2.87655667	-1.22429189	-0.24123083
H	0.27024795	4.48940360	0.41815081
H	-0.20518365	-4.49006629	-0.41539348
H	4.47281334	-0.24888434	0.17865619
S	-3.79813717	0.21756531	-0.14923826
H	2.88120092	4.35749059	0.51738005
H	4.66916365	2.34439573	0.41364155
H	4.40005242	-2.86121123	-0.05303292
H	2.41068282	-4.65967400	-0.30522497
H	-2.78192460	-4.48799593	-0.53464065
H	-4.66318058	-2.56787852	-0.44230477
H	-2.29720571	4.78468646	0.33340964
H	-4.37080359	3.08899975	0.08368050
Zn	-0.02658306	0.00114282	0.00130404

7. Excited State Dynamics

Femtosecond Transient Absorption and Transient Absorption Anisotropy

Dual-beam femtosecond time-resolved transient absorption (TA) spectrometer consisted of two independently-tunable homemade noncollinear optical parametric amplifiers (NOPA) pumped by a regeneratively amplified Ti:sapphire laser system (Spectra-Physics, Hurricane-X) operating at 3 kHz repetition rate and an optical detection system. The NOPA was based on non-collinearly phase-matching geometry, which was easily color-tuned by controlling the optical delay between white light continuum seed pulses (450-1400 nm) and visible pump pulses (400 nm) produced by using a sapphire window and BBO crystal, respectively. The generated visible OPA pulses had a pulse width of ~ 35 fs and an average power of 10 mW at 3 kHz repetition rate in the range 500-700 nm after a fused-silica prism compressor. Two OPA pulses were used as the pump and probe pulses, respectively, for TA measurement. The probe beam was split into two parts. The one part of the probe beam was overlapped with the pump beam at the sample to monitor the transient (signal), while the other part of the probe beam was passed through the sample without overlapping the pump beam to compensate the fluctuation of the probe beam. The time delay between pump and probe beams was carefully controlled by making the pump beam travel along with a variable optical delay (Newport, ILS250). To obtain the time-resolved transient absorption difference signal at a specific wavelength, the monitoring wavelength was selected by using a narrow interference filter (FWHM ~10 nm). By chopping the pump pulses at 47 Hz, the modulated probe pulses as well as the reference pulses were detected by two separate photodiodes (New Focus, Femtowatt Photoreceiver). The modulated signals of the probe pulses were measured by a gated-integrator (SRS, SR250) and a lock-in amplifier (EG&G, DSP7265) and stored in a personal computer for further signal processing. In general, experimental conditions, time-resolutions of less than 50 fs were achieved. For transient absorption anisotropy (TAA) measurement, both $I_{//}(t)$ and $I\perp(t)$ signals were collected simultaneously by a combination of polarizing beam-splitter cube and dual lock-in amplifiers as following equation:[6]

$$r(t) = [\ I_{//}(t) - I\perp(t)] \ / \ [\ I_{//} + 2I\perp(t)]$$

where $I_{//}(t)$ and $I\perp(t)$ represent TA signals with the polarization of the pump and probe pulses being mutually parallel and perpendicular, respectively. The pump pulses were set to vertical polarization and that of probe pulse was set to 45° with respect to the pump pulse by using Glan-laser polarizers and half-wave plates. After the probe pulse passes through the sample cell, it is split by polarizing beam-splitter cube and then detected by two separate photodiodes. Two gated-integrators and two lock-in amplifiers record the signal simultaneously within a single scan. A standard anisotropy measurement showed a clean single exponential decay with reorientational relaxation times of 122.1 ± 0.3 ps and the initial anisotropy r_0 value of 0.39 ± 0.02 for rhodamine 6G dye in methanol, which is well-matched with other references. For all TAA measurements, a thin absorption cell with a path length of 0.5 mm was used to eliminate additional chirping.

Picosecond time-resolved fluorescence measurements

A time-correlated single-photon-counting (TCSPC) system was used for measurements of spontaneous fluorescence decay. As an excitation light source, we used a mode-locked Ti:sapphire laser (Spectra Physics, MaiTai BB), which provides ultrashort pulse (center wavelength of 800 nm with 80 fs at FWHM) with a high repetition rate (80 MHz). This high repetition rate was reduced to 800 kHz by using a homemade pulse-picker. The pulse-picked output was frequency doubled by a 1-mm-thick BBO crystal (type-I, $\theta = 29.2°$, EKSMA). The fluorescence was collected by a microchannel plate photomultiplier (MCP-PMT, Hamamatsu, R3809U-51) with a thermoelectric cooler (Hamamatsu, C4878) connected to a TCSPC board (Becker & Hickel SPC-130). The overall instrumental response function was about 25 ps (FWHM). A vertically polarized pump pulse by a Glan-laser polarizer was irradiated to samples, and a sheet polarizer set at an angle complementary to the magic angle (54.7°), was placed in the fluorescence collection path to obtain polarization-independent fluorescence decays.

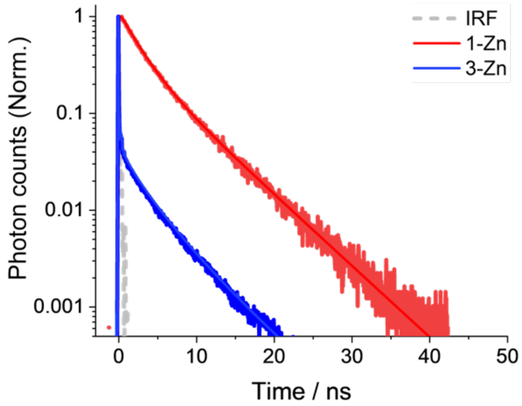

Figure S21. Fluorescence decay profiles of **1-Zn** and **3-Zn** in dichloromethane measured by TCSPC method under photoexcitation at 400 nm. The probed wavelength was selected at 700 and 680 nm, respectively.

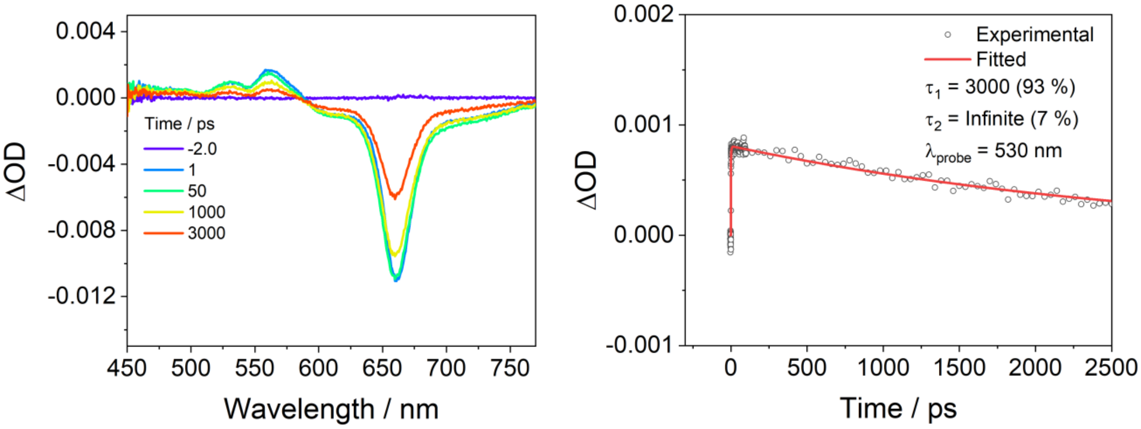

Figure S22. Femtosecond transient absorption spectra and decay profiles of **1-Zn** in dichloromethane probed at the visible region. The excitation wavelength of 660 nm is employed.

8. Decay Rate Constant Calculations

Theoretical estimation of the decay rate constants was performed on the S_1–S_0 internal conversion as well as the S_1–T_1 and S_1–T_2 intersystem crossings for **1-Zn** and **3-Zn**. We used the rate formalism based on the time-dependent perturbation theory in conjunction with the Born-Oppenheimer adiabatic framework. The task of the analysis begins with density functional theory (DFT) calculations and is followed by the rate constant calculations on top of the DFT results.

By carrying out the DFT calculations, the adiabatic potential energy surfaces of the molecules of interest were characterized, which are used for inputs to the rate constant calculations. The CAM-B3LYP functional[2] was thoroughly used. The solvation effect in dichloromethane as solvent was accounted for using the Polarizable Continuum Model (PCM) with the integral equation formalism (IEFPCM).[3] We used Gaussian 16 Revision B.01[7] for performing structural optimizations and vibrational frequency analysis and for calculating nonadiabatic coupling (NAC) and transition dipole moments. The electronically excited states, S_1, T_1, and T_2, were determined using the time-dependent DFT[8] approach with the restricted formalism and Tamm-Dancoff approximation.[9] In these calculations, the 6-311+G(2d,p)[10,11] basis sets were used except for the Zn atom, for which the SDD/StuttgartECP[12,13] was used.

The electronic state transition between the singlet and triplet manifolds is mediated by the spin-orbit coupling (SOC), which thus needs to be evaluated with the use of the electronic structure theory. The SOC matrix elements (SOCMEs) were determined at the DFT level of theory using ORCA program suite version 5.0.1.[14] In the SOC calculations, the quasi-relativistic treatment with the zero-order regular approximation (ZORA)[15] was employed. The acceleration technique RIJCOSX, as well as the SOCME treatment RI-SOMF(1X) implemented in ORCA, were exploited (see Ref. 14 for details). The ZORA-def2-TZVP basis sets combined with the SARC/J auxiliary basis sets[16] were used. We further calculated the derivatives of SOCMEs with respect to nuclear coordinates through numerical differentiation, for which a nuclear displacement of 0.001 Bohr was used. Using them in conjugation with the rate constant simulation allows us to account for vibronically induced spin-orbital coupling.

Based on information regarding the potential energy surfaces and their couplings (NACs and SOCMEs), the decay rate constants of electronic transitions were numerically simulated at the level of the time-dependent perturbation theory with the thermal vibration correlation function (TVCF) formalism.[17-20] The approach can account for origin displacement and

Duschinsky rotation within the multimode harmonic oscillator model. Its numerical simulation was performed using our in-house computer implementation. The redundant internal coordinate space was used for the normal coordinate construction.[21,22] Radiative decay transition rate (k_r) and nonradiative intersystem crossing rate (k_{isc}) were calculated through the use of transition dipole moments and SOCMEs, respectively, under the Franck-Condon (FC) and Herzberg-Teller (HT) approximations. The nonradiative internal conversion rate (k_{ic}) was estimated with the direct nonadiabatic transition term at the first-order perturbation. The NACs and SOCMEs calculated at the S_1 geometry were used in this rate simulation.

The scaling factor applied for the vibrational frequencies was not considered. The vibronic manifold at the initial state was modeled by the Boltzmann distribution with the temperature set to 300 K. For the dephasing function, the Gaussian function with its HWHM of 50 cm^{-1} was used. The integration for time to evaluate the correlation function was performed with a range of 0.05 to 10000.05 fs with a time step of 0.1 fs. The correlation function at the negative time was constructed as the complex conjugate of the positive time region.

Table S7 shows the adiabatic transition energies of the S_0, T_1, and T_2 states of compounds **1-Zn** and **3-Zn** relative to the S_1 state. The S_1 state was precited to lie all below the S_0, T_1, and T_2 states but close to the T_2 states with an energy difference of 0.206 and 0.407 eV for **1-Zn** and **3-Zn**, respectively. This hints the possibility of the ISC decay channel from S_1 to T_2 states.

In Table S8, the radiative and nonradiative decay rate constants predicted using the TVCF approach are summarized. The major decay pathway of photoexcited **1-Zn** is indicated to arise from the intersystem crossing to the T_2 state with the rate constant of 4.7×10^8 s^{-1}; nonetheless, the radiative $S_1 \rightarrow S_0$ transition for **1-Zn** plays an appreciable role as the decay channel with a rate of 1.03×10^8 s^{-1}. The rate constant of the internal conversion to the S_0 state in **3-Zn** was predicted to be 2.1×10^9 s^{-1}, suggesting that the photoexcited **3-Zn** primarily decays through the internal conversion. The radiative decay rate constant for **3-Zn** is calculated to be much smaller than the nonradiative counterparts. Interestingly, the ISC decay does not serve as a major channel for **3-Zn** despite the fact that it involves the heavier element S compared to **1-Zn**. Overall, a clear difference in the decay mechanism was quantitatively identified by our rate constant simulations.

The characterization of the excited states the S_1, T_1, and T_2 states on the basis of the natural transition orbital (NTO) analysis is shown in Figure S23. The lowest singlet (S_1) and triplet (T_1) excited states are commonly ascribed to the single-electron HOMO to LUMO excitation relative to the ground-state S_0 state of closed-shell nature. Because of these common electronic configurations, the SOCMEs between S_1 and T_1 vanish and thus the associated ISC interconversion is forbidden. The T_2 state is mainly characterized as a mixture of two excited configurations HOMO–1 → LUMO and HOMO → LUMO+1; however, the mixture ratio somehow differs between **1-Zn** and **3-Zn**.

In Figure S24, the NAC constants are plotted as a function of normal modes for **1-Zn** and **3-Zn**. Overall, they do not appear to exhibit marked differences between the two compounds. Figure S25 displays the Huang-Rhys (HR) factors as a function of normal modes. Again, the sulfur substitution of **3-Zn** seemingly does not make a large change in structural modifications arising from the vibrational quanta in the process of the S_0–S_1 transition.

It is questionable why the substitution with the S atom in **3-Zn** promotes the nonradiative internal conversion rate (k_{ic}) by six orders of magnitudes in a drastic manner compared to **1-Zn** (Table S8). We attempted to address this question by analyzing the simulated rate constants. An important finding is that the large k_{ic} of **3-Zn** may be linked to the frequency of its lowest-lying mode (22.4 cm^{-1}) associated with the out-of-plane motion of the relatively floppy sulfur atom, which is far lower than the second-lowest frequency of **3-Zn** (51.1 cm^{-1}) and the second-lowest frequency of **1-Zn** (59.2 cm^{-1}), which likewise contains the out-of-plane motion of the O atom, as shown in Figure S26. To deduce the role of the lowest frequency of **3-Zn** (i.e., 22.4 cm^{-1}), we reiterated the calculation of k_{ic} for **3-Zn** by using the value of the second-lowest frequency of **1-Zn** (i.e., 59.2 cm^{-1}) in place of the parameter 22.4 cm^{-1}. This yielded a rate constant of $2.64 \times 10^3\ \mathrm{s}^{-1}$, reproducing a large suppression of the internal conversion. Conversely, k_{ic} was recalculated for **1-Zn** by replacing its second-lowest frequency parameter (59.2 cm^{-1}) with **3-Zn**'s lowest frequency (22.4 cm^{-1}), resulting in a largely enhanced rate constant ($4.42 \times 10^9\ \mathrm{s}^{-1}$), which can more or less simulate large k_{ic} of **3-Zn**. This analysis strongly indicates that the presence of the relatively low frequency, 22.4 cm^{-1}, in the initial state plays a key role in a remarkable enhancement of the internal conversion decay from S_1 to S_0 in **3-Zn**.

Table S7. Predicted relative energies (in eV) of the S_0, T_1, and T_2 states of compounds **1-Zn** and **3-Zn** with respect to the S_1 state at the TDA-RCAM-B3LYP level of theory. The state energies were calculated using the optimized structures for the corresponding states.

	1-Zn	**3-Zn**
S_0	–2.203	–2.189
T_1	–0.899	–0.841
T_2	–0.206	–0.407

Table S8. Radiative decay rate constants k_r (in s^{-1}) from the first excited state S_1 to the ground state S_0, nonradiative decay rate constants associated with intersystem crossing k_{isc} (in s^{-1}) for S_1 to T_1 and T_2 states and internal conversion k_{ic} (in s^{-1}) for S_1 to S_0 simulated for compounds **1-Zn** and **3-Zn**.

	1-Zn	**3-Zn**
Radiative transition		
k_r ($S_1 \rightarrow S_0$)	1.03×10^8	9.26×10^7
Nonradiative transition		
k_{isc} ($S_1 \rightarrow T_1$)	4.51×10^2	3.55×10^3
k_{isc} ($S_1 \rightarrow T_2$)	4.68×10^8	9.59×10^8
k_{ic} ($S_1 \rightarrow S_0$)	1.95×10^3	2.06×10^9

(a) **1-Zn**

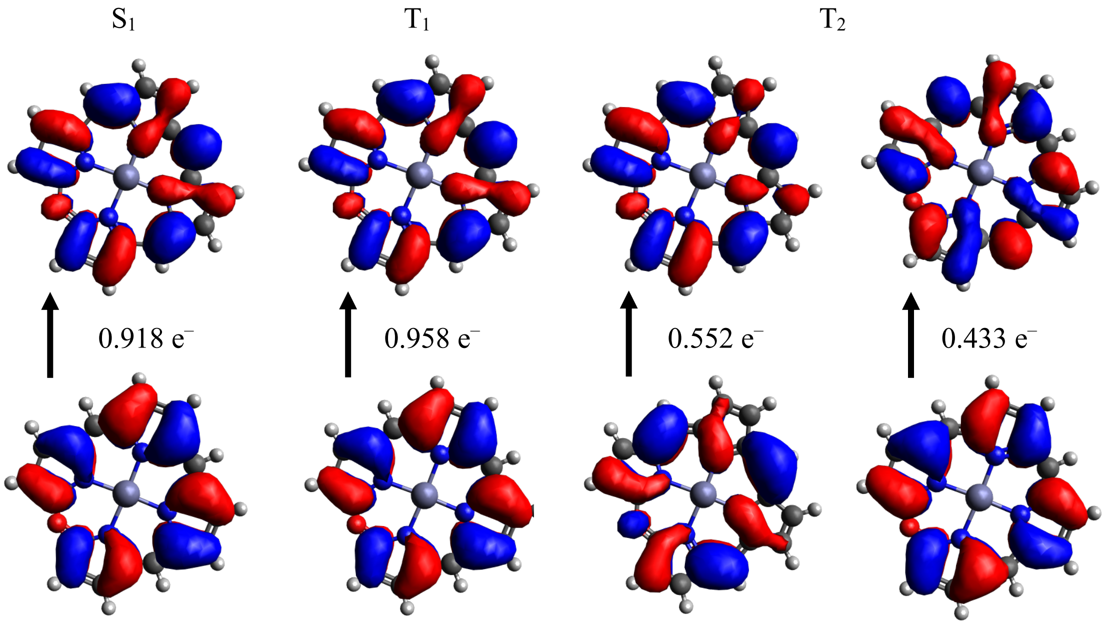

(b) **3-Zn**

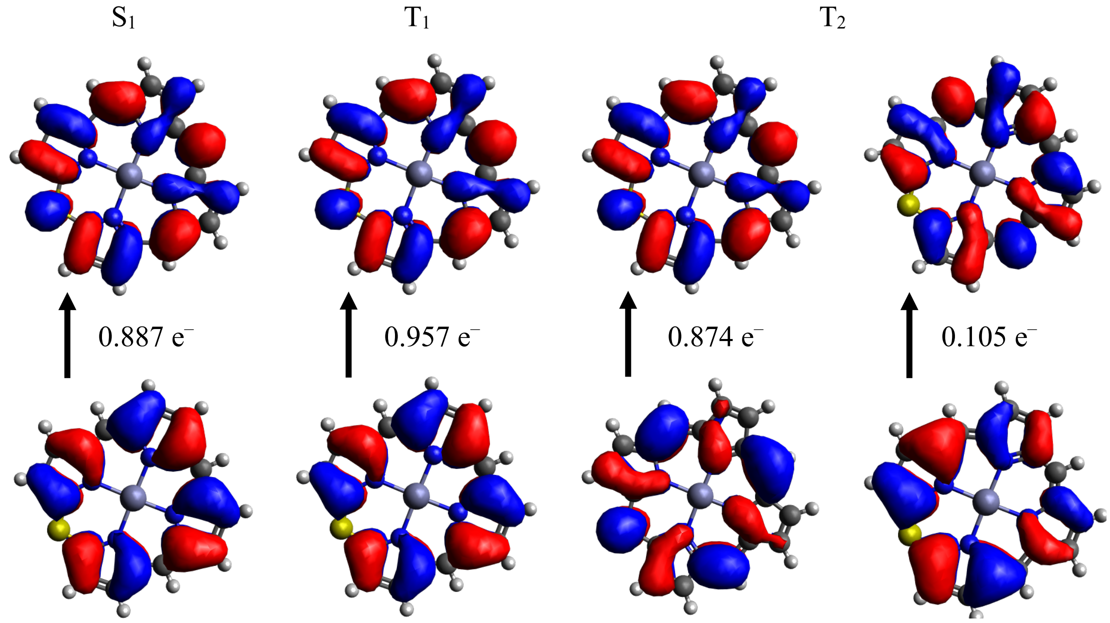

Figure S23. Electronic character of the S_1, T_1, T_2 states analyzed by natural transition orbital (NTO) method applied to compounds (a) **1-Zn** and (b) **3-Zn** at the optimized S_1 structure.

(a) **1-Zn**

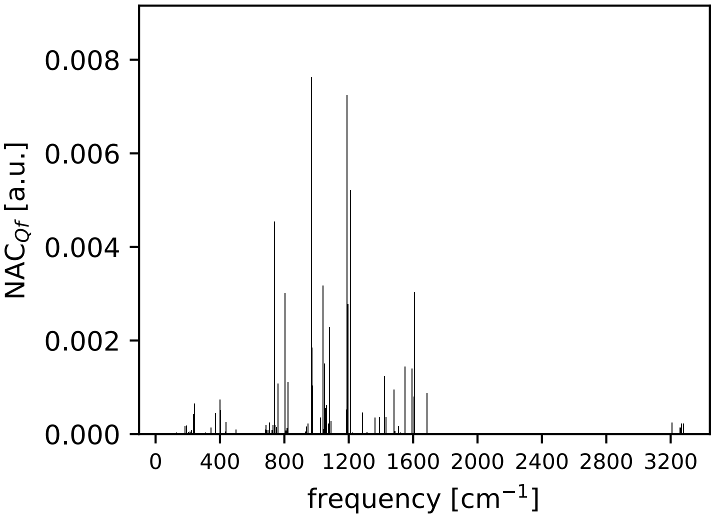

(b) **3-Zn**

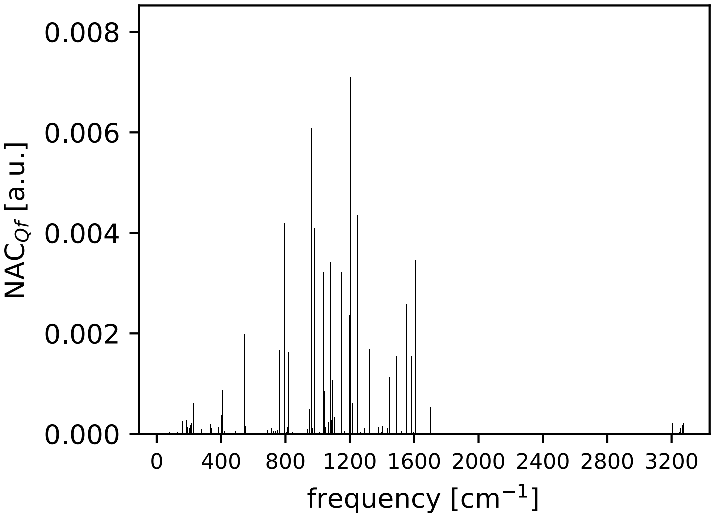

Figure S24. Nonadiabatic coupling constants between the S_0 and S_1 states obtained from TDDFT calculations as a function of normal modes at the S_0 state for compounds (a) **1-Zn** and (b) **3-Zn**.

(a) **1-Zn**

$E^{reorg} = 424\ cm^{-1}$

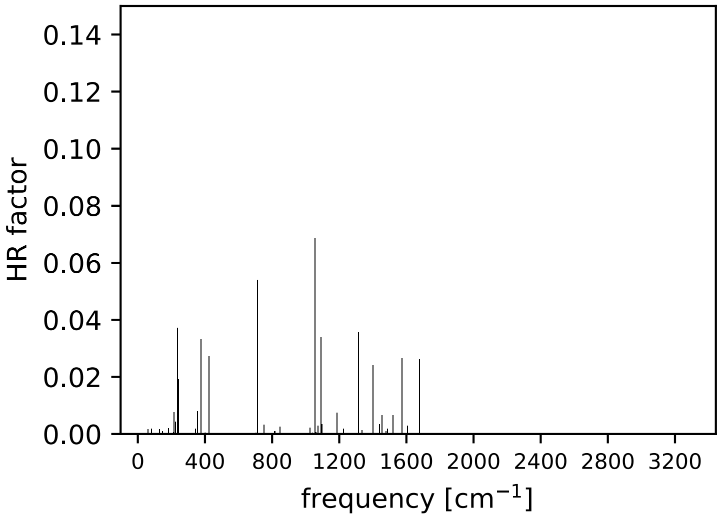

(b) **3-Zn**

$E^{reorg} = 400\ cm^{-1}$

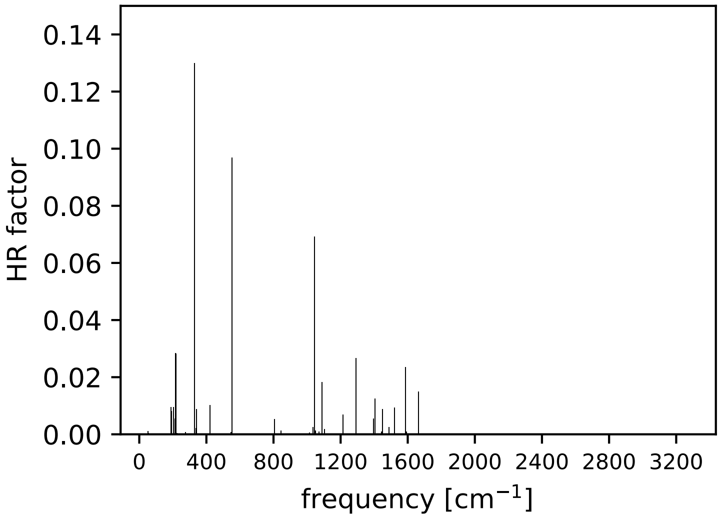

Figure S25. Huang-Rhys factors in S_1–S_0 internal conversion as a function of normal modes at the S_0 state calculated for compounds (a) **1-Zn** and (b) **3-Zn**. The total reorganization energies E^{reorg} were calculated to be 424 and 400 cm^{-1} for **1-Zn** and **3-Zn**, respectively, at the S_0 state PES.

(a) **1-Zn**

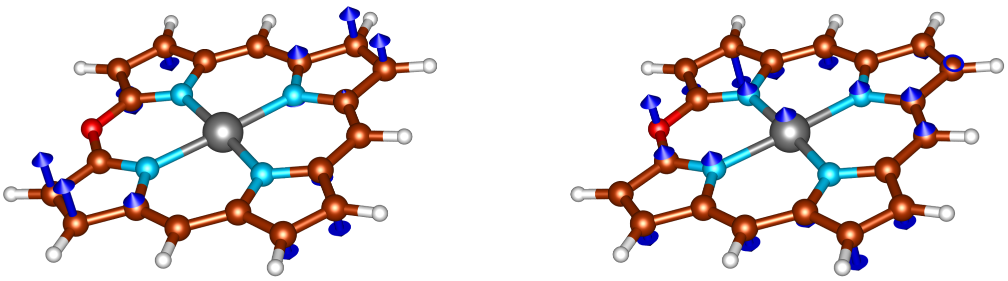

No. 1, 58.2 cm^{-1}

No. 2, 59.2 cm^{-1}

(b) **3-Zn**

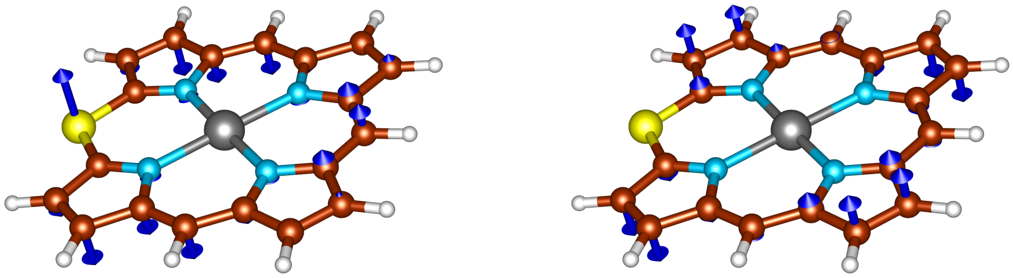

No. 1, 22.4 cm^{-1}

No. 2, 51.1 cm^{-1}

Figure S26. The displacement vectors of the two lowest-lying vibration modes in the S_1 state for (a) **1-Zn** and (b) **3-Zn**.

9. Plausible reaction pathway

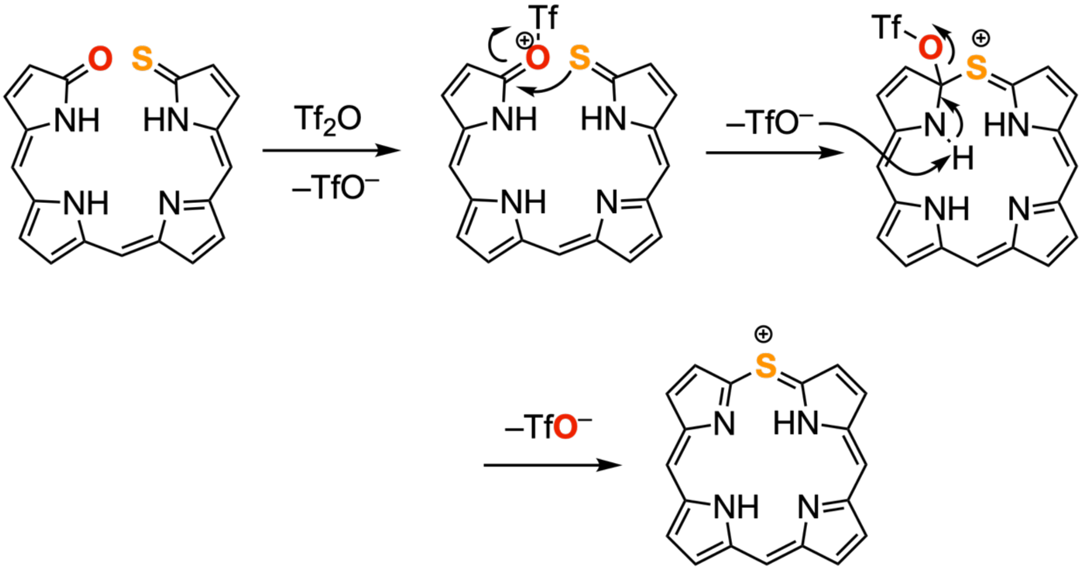

Scheme S1. Plausible reaction pathway of **3-2H**.

10. References

1. Frisch, M. J.; Trucks, G. W.; Schlegel, H. B.; Scuseria, G. E.; Robb, M. A.; Cheeseman, J. R.; Scalmani, G.; Barone, V.; Mennucci, B.; Petersson, G. A.; Nakatsuji, H.; Caricato, M.; Li, X.; Hratchian, H. P.; Izmaylov, A. F.; Bloino, J.; Zheng, G.; Sonnenberg, J. L.; Hada, M.; Ehara, M.; Toyota, K.; Fukuda, R.; Hasegawa, J.; Ishida, M.; Nakajima, T.; Honda, Y.; Kitao, O.; Nakai, H.; Vreven, T.; Montgomery, J. A., Jr.; Peralta, J. E.; Ogliaro, F.; Bearpark, M.; Heyd, J. J.; Brothers, E.; Kudin, K. N.; Staroverov, V. N.; Kobayashi, R.; Normand, J.; Raghavachari, K.; Rendell, A.; Burant, J. C.; Iyengar, S. S.; Tomasi, J.; Cossi, M.; Rega, N.; Millam, J. M.; Klene, M.; Knox, J. E.; Cross, J. B.; Bakken, V.; Adamo, C.; Jaramillo, J.; Gomperts, R.; Stratmann, R. E.; Yazyev, O.; Austin, A. J.; Cammi, R.; Pomelli, C.; Ochterski, J. W.; Martin, R. L.; Morokuma, K.; Zakrzewski, V. G.; Voth, G. A.; Salvador, P.; Dannenberg, J. J.; Dapprich, S.; Daniels, A. D.; Farkas, O.; Foresman, J. B.; Ortiz, J. V.; Cioslowski, J.; Fox, D. J. *Gaussian 09*, revision E.01; Gaussian, Inc.: Wallingford, CT, 2009.
2. Yanai, T.; Tew, D. P.; Handy, N. C. *Chem. Phys. Lett.* **2004**, *393*, 51–57.
3. Tomasi, J.; Mennucci, B.; Cammi, R. Quantum Mechanical Continuum Solvation Models. *Chem. Rev.* **2005** *105*, 2999–3094.
4. Takiguchi, A.; Sakakibara, E.; Sugimoto, H.; Shoji, O.; Shinokubo, H. A Heme-Acquisition Protein Reconstructed with a Cobalt 5-Oxaporphyrinium Cation and Its Growth-Inhibition Activity Toward Multidrug-Resistant *Pseudomonas aeruginosa*. *Angew. Chem. Int. Ed. in press*. https://doi.org/10.1002/anie.202112456.
5. Takiguchi, A.; Kang, S.; Fukui, N.; Kim, D.; Shinokubo, H. Dual Emission of a Free-Base 5-Oxaporphyrinium Cation from its *cis*-and *trans*-NH Tautomers. *Angew. Chem. Int. Ed.* **2021**, *60*, 2915–2919.
6. Min, C.-K.; Joo, T.; Yoon, M.-C.; Kim, C. M.; Hwang, Y. N.; Kim, D.; Aratani, N.; Yoshida, N.; Osuka, A. Transient absorption anisotropy study of ultrafast energy transfer in porphyrin monomer, its direct *meso–meso* coupled dimer and trimer. *J. Chem. Phys.* **2001**, *114*, 6750–6758.
7. Frisch, M. J.; Trucks, G. W.; Schlegel, H. B.; Scuseria, G. E.; Robb, M. A.; Cheeseman, J. R.; Scalmani, G.; Barone, V.; Petersson, G. A.; Nakatsuji, H.; Li, X.; Caricato, M.; Marenich, A. V.; Bloino, J.; Janesko, B. G.; Gomperts, R.; Mennucci, B.; Hratchian, H. P.; Ortiz, J. V.; Izmaylov, A. F.; Sonnenberg, J. L.; Williams-Young, D.; Ding, F.; Lipparini, F.;

Egidi, F.; Goings, J.; Peng, B.; Petrone, A.; Henderson, T.; Ranasinghe, D.; Zakrzewski, V. G.; Gao, J.; Rega, N.; Zheng, G.; Liang, W.; Hada, M.; Ehara, M.; Toyota, K.; Fukuda, R.; Hasegawa, J.; Ishida, M.; Nakajima, T.; Honda, Y.; Kitao, O.; Nakai, H.; Vreven, T.; Throssell, K.; Montgomery, J. A., Jr.; Peralta, J. E.; Ogliaro, F.; Bearpark, M. J.; Heyd, J. J.; Brothers, E. N.; Kudin, K. N.; Staroverov, V. N.; Keith, T. A.; Kobayashi, R.; Normand, J.; Raghavachari, K.; Rendell, A. P.; Burant, J. C.; Iyengar, S. S.; Tomasi, J.; Cossi, M.; Millam, J. M.; Klene, M.; Adamo, C.; Cammi, R.; Ochterski, J. W.; Martin, R. L.; Morokuma, K.; Farkas, O.; Foresman, J. B.; Fox, D. J. *Gaussian 16*, rev. B.01; Gaussian, Inc.: Wallingford, CT, 2016.

8. Bauernschmitt, R.; Ahlrichs, R. Treatment of electronic excitations within the adiabatic approximation of time dependent density functional theory. *Chem. Phys. Lett.* **1996**, *256*, 454–464.
9. Hirata, S.; Head-Gordon, M. Time-dependent density functional theory within the Tamm–Dancoff approximation. *Chem. Phys. Lett.* **1999**, *314***,** 291–299.
10. Krishnan, R.; Binkley, J. S.; Seeger, R.; Pople, J. A. Self-consistent molecular orbital methods. XX. A basis set for correlated wave functions. *J. Chem. Phys.* **1980**, *72*, 650–654.
11. Clark, T.; Chandrasekhar, J.; Spitznagel, G. W.; Schleyer, P. V. R. Efficient diffuse function-augmented basis sets for anion calculations. III. The 3-21+G basis set for first-row elements, Li–F *J. Comput. Chem.* **1983**, *4*, 294–301.
12. Martin, J. M. L.; Sundermann, A. Correlation consistent valence basis sets for use with the Stuttgart–Dresden–Bonn relativistic effective core potentials: The atoms Ga–Kr and In–Xe. *J. Chem. Phys.* **2001**, *114*, 3408–3420.
13. Dolg, M.; Wedig, U.; Stoll, H.; Preuss, H. A picosecond photon echo study of a chromophore in an organic glass: Temperature dependence and comparison to nonphotochemical hole burning. *J. Chem. Phys.* **1987**, *86*, 866–872.
14. Neese, F.; Wennmohs, F.; Becker, U.; Riplinger, C. The ORCA quantum chemistry program package. *J. Chem. Phys.* **2020**, *152*, 224108.
15. Lenthe, E.; Baerends, E. J.; Snijders, J. G. Relativistic regular two-component Hamiltonians. *J. Chem. Phys.* **1993**, *99*, 4597–4610.
16. Pantazis, D. A.; Neese, F. All-electron basis sets for heavyelements. *Wiley Interdiscip. Rev. Comput. Mol. Sci.* **2014**, *4*, 363–374.
17. Niu, Y.; Peng, Q.; Deng, C.; Gao, X.; Shuai, Z. Theory of Excited State Decays and Optical Spectra: Application to Polyatomic Molecules. *J. Phys. Chem. A* **2010**, *114*, 7817–7831.

18. Peng, Q.; Niu, Y.; Shi, Q.; Gao, X.; Shuai, Z. Correlation Function Formalism for Triplet Excited State Decay: Combined Spin–Orbit and Nonadiabatic Couplings. *J. Chem. Theory Comput.* **2013**, *9*, 1132–1143.
19. Etinski, M.; Tatchen, J.; Marian, C. M. Time-dependent approaches for the calculation of intersystem crossing rates. *J. Chem. Phys.* **2011**, *134*, 154105.
20. Etinski, M.; Rai-Constapel, V.; Marian, C. M. Time-dependent approach to spin-vibronic coupling: Implementation and assessment. *J. Chem. Phys.* **2014**, *140*, 114104.
21. Cerezo, J.; Zuniga, J.; Requena, A.; Avila Ferrer, F. J.; Santoro, F. Harmonic Models in Cartesian and Internal Coordinates to Simulate the Absorption Spectra of Carotenoids at Finite Temperatures. *J. Chem. Theory Comput.* **2013**, *9*, 4947–4958.
22. Baiardi, A.; Bloino, J.; Barone, V. General formulation of vibronic spectroscopy in internal coordinates. *J. Chem. Phys.* **2016**, *144*, 084114.